6

Global Bifurcation Analysis in Laser Systems

Sebastian M Wieczorek

Mathematics Research Institute, University of Exeter, United Kingdom

Nonlinear dynamics of lasers has been a lively theoretical and experimental field since the invention of the laser in 1960. Its focus in the last two decades have been instabilities in widely used semiconductor lasers. Nonlinear studies of laser systems contributed to the field of dynamical systems with general phenomena including chaos, (chaotic) synchronization of coupled oscillators, competition, excitability, delay-induced instabilities, unfolding of high-codimension bifurcations, bifurcation cascades, and spatial patterns; see [1, 28, 30, 36, 51, 63] for general reading and further references. These studies also deepened the understanding of nonlinear phenomena that are important for technological applications, e.g. external-modulation response of semiconductor lasers for faster Internet connections [57]. Furthermore, nonlinear analysis of laser systems stimulated and helped to validate the feasibility of novel, chaos-based applications including secure communication schemes [4, 50], chaotic radars [34], and instability-based laser sensors [56].

Much of the recent progress in the field of laser dynamics is owing to the application of numerical continuation techniques. The study of lasers with tools from bifurcation theory started already in 1987 with the work of Maloney and coworkers on the nonlinear dynamics of three-level molecular lasers [37]. By now, there are over one hundred publications where tools from bifurcation theory are used to investigate dynamics of various laser systems. To explain the strong impact that numerical continuation techniques had and are still having on the field of nonlinear laser dynamics we mention here four key properties that we found to be very influential in our research. Namely, numerical continuation techniques:

1. facilitate immensely the systematic search of an extensive and many-dimensional parameter space to identify the important contributions. Interesting phenomena may be missed by the traditional approach of simulation of the governing equations by direct time integration. Indeed, numerical continuation supplements numerical simulation by enabling parameter

studies to be performed to the necessary detail and accuracy, and with relatively modest computational resources;
2. allow the study of global homoclinic and heteroclinic bifurcations, which are often associated with interesting nonlinear effects but cannot be studied otherwise;
3. supplement and expand analytical bifurcation studies, which are themselves invaluable but generally restricted to small neighborhoods of parameter space, for example, near isolated individual bifurcations. Numerical bifurcation analysis is the tool of choice for those problems that cannot be addressed with analytical techniques but are of great importance to physicists, chemists, biologists, and engineers. For example, using the analytical results on bifurcation curves expected near a codimension-two bifurcation point, continuation techniques give answers to questions such as where these bifurcation curves go and to which other codimension-two bifurcation points they connect. Do phenomena occupy regions of the parameter space that can be experimentally detectable or that are of any practical interest? From a more general bifurcation theory point of view, this question concerns a better understanding of the organizing properties of bifurcations;
4. may actually stimulate real laser experiments where bifurcation diagrams are used as 'road maps' to guide experimentalists through the complexity and variety of nonlinear laser dynamics.

The aim of this chapter is to give a taste of how continuation techniques can be used to understand complicated dynamics in laser systems. At the same time, laser systems emerge as natural candidates to study how global bifurcation phenomena manifest themselves in a real system. In this sense, this chapter should also be seen as a contribution to the wider field of dynamical systems. Specifically, we present here the following two concrete examples of a global bifurcation analysis in semiconductor laser systems.

- In Sect. 6.1 we consider structures of global n-homoclinic bifurcations that lead to the phenomenon of multi-pulse excitability in semiconductor lasers with optical injection [58, 62, 64]; and
- in Sect. 6.2 we present the backbone of the bifurcation set for two back-to-back coupled lasers in which we find the counter-intuitive appearance of chaos at practically vanishing coupling [53, 54].

Both examples feature interesting global bifurcation structures that have a physical meaning and actually stimulated real laser experiments. The word 'global' in this context refers to objects in phase space that are due to certain arrangements of stable and unstable invariant manifolds, as well as to associated bifurcation structures in parameter space. In terms of the parameter space we use the physically motivated approach of calculating k-parameter bifurcation sets (usually for $k = 2$) for several fixed values of an additional $(k + 1)$st parameter. These k-dimensional bifurcation sets, which consist of

various local and global bifurcations, are slices that are influenced or even determined by unfoldings of certain codimension-$(k+1)$ bifurcations or singularities. These so-called organizing centers provide links between various types of bifurcations that appear at first glance to be (and are often thought of as) unrelated. While analytical techniques typically force investigators to focus on particular bifurcations, which imposes some sense of isolation of the particular phenomenon under investigation, numerical bifurcation analysis allows one to connect seemingly unrelated pieces. The goal is to get to a deeper understanding of the dynamics by obtaining a consistent and global bifurcation picture of the given (laser) system; see also Chaps. 2 and 7.

6.1 Multi-Pulse Excitability and n-Homoclinic Orbits in an Optically Injected Laser

This section is based on [58] and describes intricate structures of n-homoclinic orbits and their bifurcations in the rate equation model of an injection laser. The analysis reveals how codimension-two and -three homoclinic bifurcations act as organizing centers of the bifurcation diagram. First, we find heteroclinic cycles known as T-point bifurcations; we are dealing here with the case that both saddles involved have a pair of complex conjugate eigenvalues. Such T-point bifurcations were found in systems from applications [2, 19, 20, 22, 26, 32, 47, 68] and their unfolding is known to involve n-homoclinic orbits for any n [9, 10]. Secondly, we find double-homoclinic orbits to a saddle-focus, where there are two different homoclinic connections to a single saddle-focus. (This should not be confused with a 2-homoclinic orbit.) This codimension-two global bifurcation has been studied in an abstract setting in [27, 40, 44]. The bifurcations of 1-homoclinic orbits are known, but the possible unfoldings are not yet fully understood. We present sketches of relevant bifurcation curves associated with these global bifurcations and show with numerical bifurcation diagrams how they manifest themselves in the optically injected laser model. Also, we explain how these n-homoclinic bifurcations give rise to the phenomenon of multi-pulse excitability.

All curves of global bifurcations and the associated homoclinic and heteroclinic orbits were calculated with the HomCont [11, 12] part of the continuation package Auto [16]; the invariant manifolds and time series illustrating multi-pulse excitability were computed with the package DsTool [5].

6.1.1 Optically Injected Laser

From the dynamical systems point of view, a free-running class-B laser (the active-medium polarization decays much faster than the population inversion and electric field) is a damped nonlinear oscillator characterized by a stable equilibrium with two complex-conjugate eigenvalues. This situation can be changed drastically when the laser is subjected to an external optical signal,

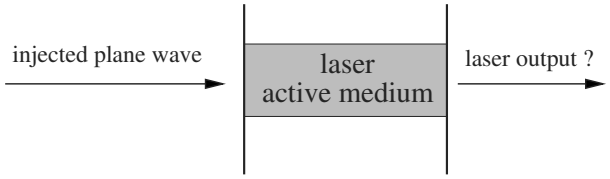

Fig. 6.1. A laser that is being injected with an external optical field.

as discussed here and sketched in Fig. 6.1. With optical injection it becomes a driven nonlinear oscillator: one of the nicest physical systems to show a fascinating array of nonlinear dynamics. Several kinds of complex and chaotic dynamics were discovered; see, for example, [3, 17, 21, 35, 29, 59, 63]. Of particular importance is the fact that this system is very well described by a set of three autonomous ordinary differential equations for the complex electric field $E = E_x + iE_y$ and the population inversion n (the number of electron-hole pairs in the case of a semiconductor laser) [48, 59]. These so-called *single-mode rate equations* for this system can be written in dimensionless form as

$$\begin{cases} \dot{E} = K + \left(\frac{1}{2}(1+i\alpha)n - i\omega\right) E \\ \dot{n} = -2\Gamma n - (1+2Bn)(|E|^2 - 1) \ . \end{cases} \tag{6.1}$$

The two main parameters are the injected field amplitude K and the detuning ω, the frequency difference between the injected light and the frequency of the laser without injection. The explicit time dependence in the drive term proportional to K was eliminated thanks to the S^1 symmetry of the system [63]. While K and ω can easily be changed in an experiment, the parameters B, Γ and α describe material properties of a given laser. Specifically, B is the rescaled lifetime of photons in the laser cavity and Γ is the rescaled damping rate of the so-called relaxation oscillations, which are an exchange of energy between the electric field E and the population n of a characteristic frequency ω_R in a free-running laser. We use the realistic values $B = 0.015$ and $\Gamma = 0.035$ throughout in our study.

The material constant α, called the *linewidth enhancement factor*, can be very different for different lasers, and it is known that changing α has a very large effect on the dynamics of the injected laser [59]. The parameter α describes the coupling between the phase and the amplitude of the electric field E, and it is in the range of $\alpha \in [1, 10]$ for typical semiconductor lasers. On the other hand, (6.1) for $\alpha = 0$ models injected solid-state and CO_2 lasers, which have a negligible phase-amplitude coupling. This is our motivation for studying how the bifurcation set in the (K, ω)-plane depends on α, that is, on the main material property of the particular laser under consideration.

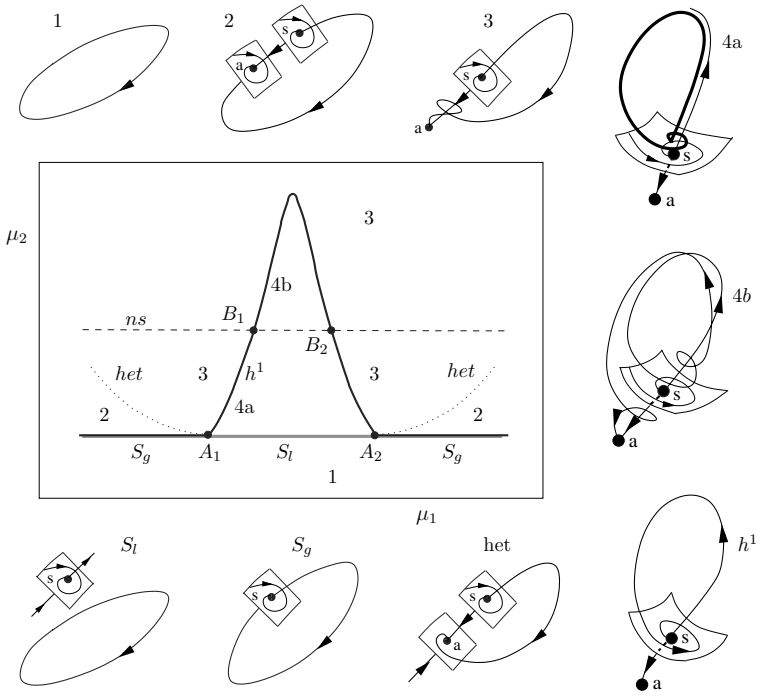

Fig. 6.2. Sketches of phase portraits near the boundary of a homoclinic tooth in two unfolding parameters μ_1 and μ_2. From S. Wieczorek and B. Krauskopf, Bifurcations of n-homoclinic orbits in optically injected lasers, *Nonlinearity* 18(3) (2005) 1095–1120 © 2005 by Institute of Physics Publishing; reprinted with permission.

6.1.2 Homoclinic Teeth

The phenomena we are interested in appear in what we call 'homoclinic teeth'. What we mean by a homoclinic tooth is sketched in Fig. 6.2. It is the region bounded by the curve h^1 of a 1-homoclinic bifurcation and the grey part of the curve S_l of local saddle-node bifurcations. The two curves meet at two points A_1 and A_2 of codimension-two non-central saddle-node homoclinic bifurcations. This codimension-two bifurcation was identified in [31] as an organizing center for multi-pulse excitability (single pulse excitability in this case of a curve of 1-homoclinic bifurcations); see [6, 14, 15] for more details on its unfolding. Figure 6.2 shows sketches of phase portraits for different locations of parameter space near the homoclinic tooth. Notice, in particular, that the saddle-node bifurcation takes place on a periodic orbit along the parts marked S_g (where g stands for global), but this is not the case along S_l (where l stands for local).

In the part of region 3 that is close to the curves h^1 and S_g the laser is 1-excitable: a small perturbation to above the stable manifold of the saddle s will lead to a large excursion, which follows the one-dimensional unstable manifold

of s, before the laser relaxes back to the attractor a. By comparison, in region 2 there is a smooth invariant circle, but the laser is still excitable close to the curve S_g: a perturbation beyond the stable manifold of s will lead to a large excursion around the invariant circle and back to a. In fact, phase portraits 2 and 3 are topologically equivalent. However, away from the codimension-two points A, they may relate to different physical phenomena. On the one hand, phase portrait 2 represents phase locking because the smooth invariant circle is centered at the origin of the complex E-plane. Hence, an excitable response associated with phase portrait 2 is mainly of the form of a 2π phase slip with only slight variations in the electric field intensity. On the other hand, the upper branch of the unstable manifold in phase portrait 3 evolves away from the origin of the complex E-plane so that an excitable response leads to a short (30 ps in our case) and distinct intensity pulse. Near A, the difference in the excitable response for the phase portraits 2 and 3 disappears. The curve *het* is not a bifurcation curve, but when crossing it there is a change of the direction from which the relevant branch of the unstable manifold of the saddle approaches the attractor. Consequently, the closure of the unstable manifold of the saddle is a smooth curve in region 2, while this is not the case in region 3; see [31] for more details.

The homoclinic tooth is shown to intersect with the dashed curve ns where the saddle is neutral, that is, the absolute values of the real parts of the real eigenvalue and of the pair of complex conjugate eigenvalues are equal. What the dynamics looks like inside the tooth crucially depends on whether one is above or below ns. Along the parts of h^1 below ns, often called a simple Shil'nikov case, the homoclinic orbit bifurcates into an attracting periodic orbit [Fig. 6.2(4a)]. On the other hand, along the parts of h^1 above ns, often called a chaotic Shil'nikov case, the bifurcating periodic orbit is no longer stable [Fig. 6.2 (4b)]. Breaking this type of homoclinic orbit leads to the creation of n-homoclinic orbits for any n. While the curve ns is not a bifurcation curve, each of its intersection points B_1 and B_2 with h^1 is a codimension-two homoclinic bifurcation, known as a Belyakov point [7, 24]. Belyakov points mark the transition between the two cases of homoclinic orbits and, hence, give rise to an intricate structure of n-homoclinic orbits.

How homoclinic teeth arise in (6.1) is shown in Fig. 6.3 with panels of the (K, ω)-plane of (6.1) near the locking region for increasing values of α as indicated. It shows the curves S of saddle-node bifurcations and the curves H of Hopf bifurcations (both gray), the supercritical parts of which bound the locking region of the injected laser; see [59]. Also shown is the neutral saddle curve ns. All these curves are given by local conditions at equilibria of (6.1) and can be found analytically. The curve h^1 of 1-homoclinic bifurcations, on the other hand, cannot be found analytically. It was computed with the AUTO/HOMCONT. The computations do not distinguish between a generic (codimension-zero) homoclinic connection along the parts S_g in Fig. 6.2 and the codimension-one homoclinic bifurcation along h^1. In other words, when the

bold black curve in Fig. 6.3 coincides with S then the saddle-node bifurcation takes place on a periodic orbit. If it leaves S we find a homoclinic tooth.

For $\alpha = 0$ (the case of a solid-state or CO_2 laser) the (K, ω)-plane is symmetric and there are no homoclinic teeth. As α is increased, homoclinic teeth start to grow along the saddle-node bifurcation curve S that forms the lower boundary of the locking range. (The other boundary is the Hopf bifurcation curve H.) Initially the teeth are quite small [panels (b)–(c)] but then they grow in size with α and the bifurcation diagram changes qualitatively, showing the existence of codimension-three phenomena. At $\alpha = 1.21$ [panel (c)] the first tooth starts to intersect the neutral saddle curve ns. What is more, new teeth start to appear between already present teeth [panel (e)]. All teeth keep growing, and the tooth closest to the saddle-node Hopf point G_1 develops a rather bizarre shape [panels (f)–(i)]. On top of this, when α increases neighboring teeth may merge, meaning that the curve h^1 detaches from the curve S. This occurs at codimension-three points when two neighboring non-central saddle-node homoclinic bifurcation points come together and vanish. Furthermore, one notices the appearance of codimension-two homoclinic bifurcation points (dots along the curve h^1 in panels (h) and (i)). They are created when the section given by fixed α crosses a minimum in the respective codimension-two bifurcation curve, which is discussed in detail in Sect. 6.1.5.

To study how new teeth are born and neighboring teeth merge we continued with HomCont the curve of codimension-two non-central saddle-node homoclinic bifurcations in (K, ω, α)-space [6, 45]. The projection of this curve onto the (α, ω)-plane is shown in Fig. 6.4(a), while Fig. 6.4(b) shows a sketch of a non-central saddle-node homoclinic orbit. The left-hand fold points of the curve in Fig. 6.4(a) are points where teeth are born, while right-hand fold points are points where two neighboring teeth merge. This figure clearly shows that there are no teeth for $\alpha < 0.5$. New teeth are then born one-by-one as α is increased. Secondary teeth appear from about $\alpha = 2$ on. Merging teeth can be observed from about $\alpha = 2.2$ onward when the first two teeth (nearest G_1) merge. Successively teeth for larger negative detuning ω also merge. In fact for $\alpha > 7.5$ there appears to be one giant tooth, if one still wants to call it that. It is already clear that the situation becomes increasingly complicated with α.

6.1.3 Complex Structure of n-Homoclinic Bifurcations

Complex structures of global homoclinic and heteroclinic bifurcations arise inside the homoclinic teeth as a result of interactions of the curves of 1-homoclinic orbits. The fact that the curve ns intersects the first homoclinic tooth, for example, for $\alpha = 2.0$ in Fig. 6.3 (d), giving rise to two Belyakov points, already allows us to conclude from general theory [7, 24] that there must be further curves of n-homoclinic orbits. We remark that the exact combinatorics of these n-homoclinic orbits is still not fully understood [24].

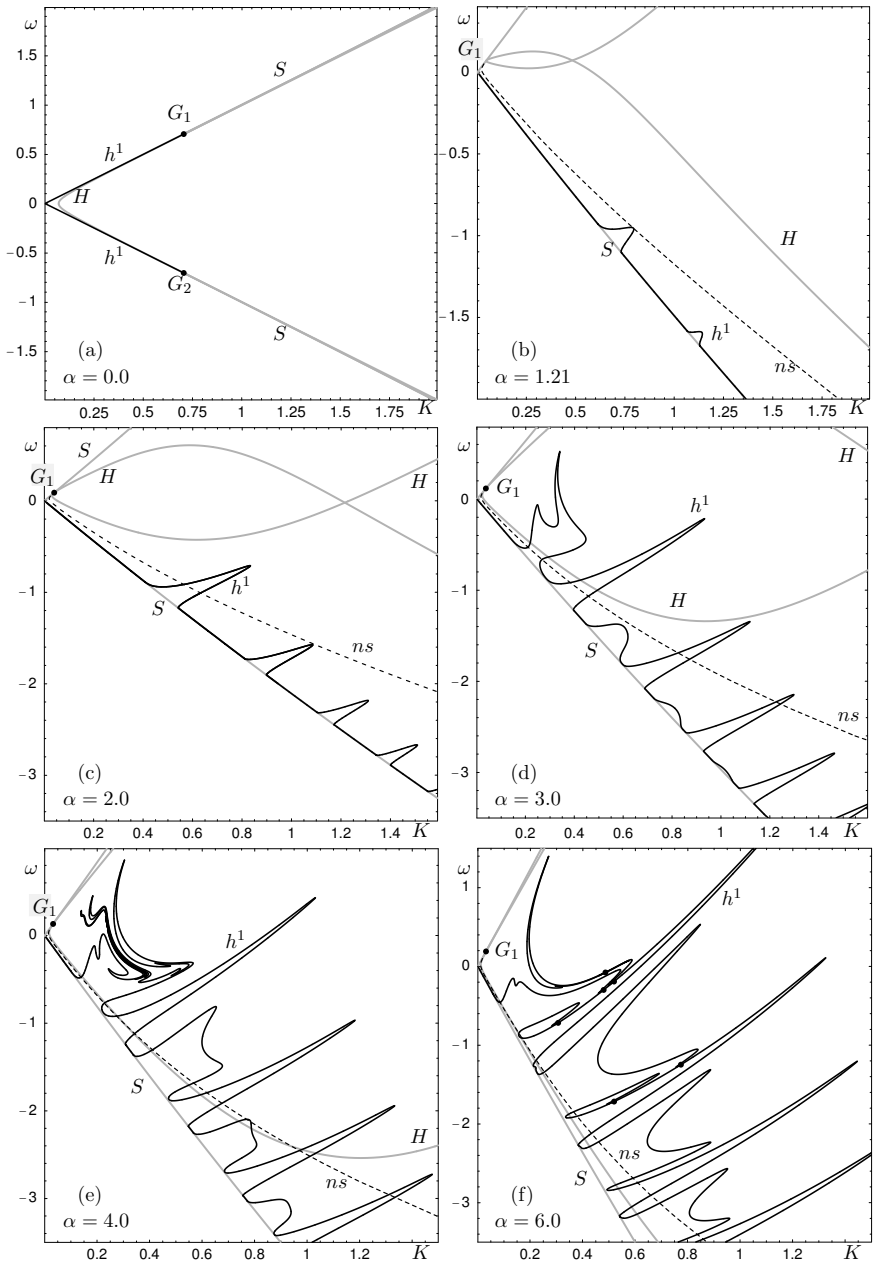

Fig. 6.3. Homoclinic teeth in the locking region as a function of α. From S. Wieczorek and B. Krauskopf, Bifurcations of n-homoclinic orbits in optically injected lasers, *Nonlinearity* 18(3) (2005) 1095–1120 © 2005 by Institute of Physics Publishing; reprinted with permission.

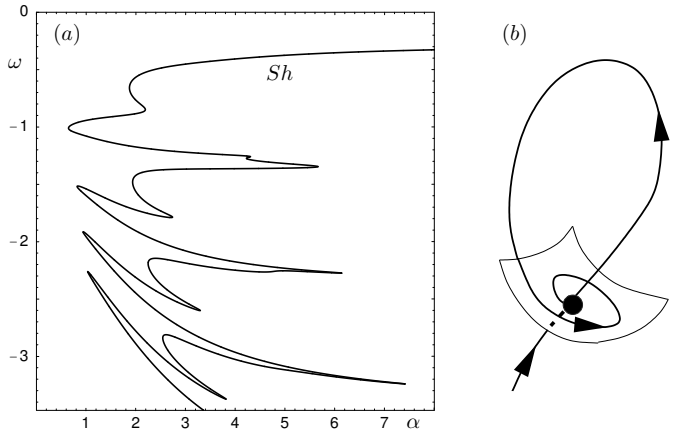

Fig. 6.4. Curve of codimension-two saddle-node homoclinic bifurcations, projected onto the (α, ω)-plane (a), and a sketch of a codimension-two saddle-node homoclinic orbit (b). From S. Wieczorek and B. Krauskopf, Bifurcations of n-homoclinic orbits in optically injected lasers, *Nonlinearity* 18(3) (2005) 1095–1120 © 2005 by Institute of Physics Publishing; reprinted with permission.

The question is how these n-homoclinic orbits are organized inside the homoclinic teeth. At the same time, we obtain an impression of a Belyakov bifurcation in a concrete system. Furthermore, one may ask where the associated n-homoclinic bifurcation curves go and to which other codimension-two points they connect. In short: what is the bifurcation diagram, as far as one can assemble it? These questions cannot be addressed by analytical studies in a neighborhood near codimension-two points but they require the use of continuation techniques. From a bifurcation theory point of view, this is the next step towards the understanding of the organizing properties of global bifurcations. Physically, we reveal structures that stretch over large regions in the parameter plane and become experimentally accessible, that is, potentially relevant for real applications of optically injected lasers.

Figure 6.5 (a1) shows curves h^n of n-homoclinic orbits for $n \leq 4$ inside the first tooth for $\alpha = 2.0$, while Fig. 6.5 (a2) is an enlargement near the saddle-node bifurcation curve S. Many of these curves extend from the region above ns to below ns and in crossing ns have further Belyakov points on them. The picture that emerges is that of a complicated arrangement of nested n-homoclinic bifurcation curves. Most interestingly, several curves extend to very near the curve S, and some even attach to S at points of non-central saddle-node n-homoclinic orbits.

We now focus on what happens to the infinite number of h^n-tongues when the Belyakov points are gone, that is, the homoclinic tooth is entirely below the curve ns. One straightforward scenario would be that all the h^n curves disappear when B_1 and B_2 merge. However, this is not the case here. Fig-

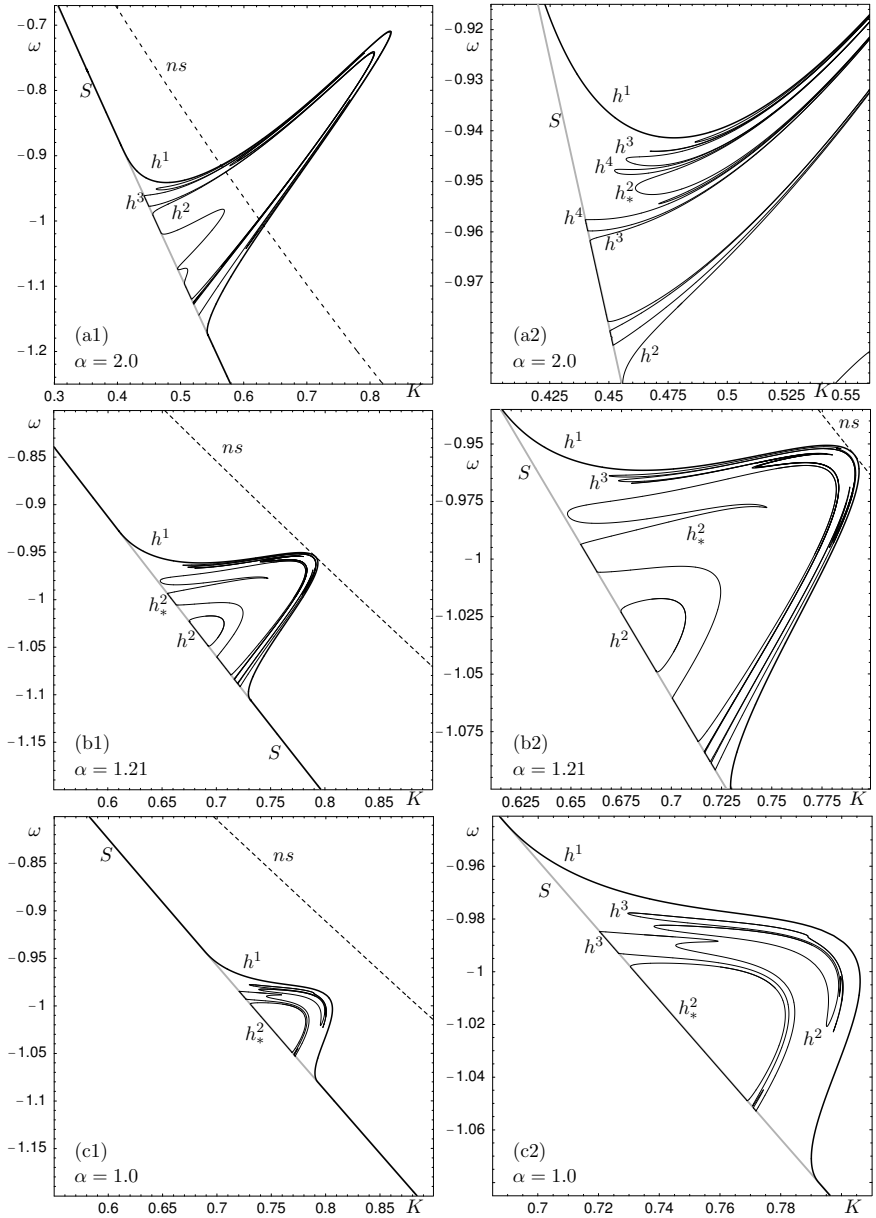

Fig. 6.5. Bifurcation curves of n-homoclinic curves inside a homoclinic tooth for three different values of α as indicated in the panels. From S. Wieczorek and B. Krauskopf, Bifurcations of n-homoclinic orbits in optically injected lasers, *Nonlinearity* 18(3) (2005) 1095–1120 © 2005 by Institute of Physics Publishing; reprinted with permission.

ure 6.5 (b1)–(b2) shows the first tooth for $\alpha = 1.21$, just as it touches the curve ns. This is a codimension-three phenomenon in (K, ω, α)-space where two Belyakov points coincide and then disappear when α is decreased, as is shown in Fig. 6.5 (c1)–(c2). (The curve B of Belyakov points in (K, ω, α)-space has a minimum.) Even though the tooth is well below the curve ns for $\alpha = 1.0$, there are still curves of n-homoclinic orbits inside it. In particular, we find that the curves h^2 and h^3 are attached to S.

Our numerical investigation suggests that there are only finitely many curves of n-homoclinic orbits for $\alpha < 1.21$. To illustrate how subsequent curves h^n appear with increasing α we marked one of them with a star. For $\alpha = 1.0$ [Fig. 6.5 (c2)] h^2_* is the last homoclinic curve that just emerged from the saddle-node bifurcation curve S. As α is increased above $\alpha = 1.0$, the curve h^2_* develops two extra noncentral-homoclinic points on S, forms a sort of bridge, and provides space for the next homoclinic curve to emerge [Fig. 6.5 (b2)]. This process seems to repeat, such that for $\alpha > 1.21$ there exist infinitely many curves h^n.

6.1.4 Multi-Pulse Excitability

The regions bounded by h^2 and h^3 near S appear to be large enough to be experimentally accessible [60]. In such a region the laser exhibits multi-pulse excitability. We remark that our study shows that this phenomenon can be found even for surprisingly low values of α; see also [31, 62]. An example is shown in Fig. 6.6 for $\alpha = 1.0$. The phase portrait in Fig. 6.6 (a1) is as that of region 3 in Fig. 6.2 — the laser is 1-pulse excitable. A small perturbation above the excitability threshold, given by the stable manifold of the saddle point, results in the laser sending out a single pulse; see Fig. 6.6 (a2). In the region bounded by h^2, on the other hand, the phase portrait is close to a 2-homoclinic orbit and the laser produces two pulses in reaction to a single perturbation; see Fig. 6.6 (b1)–(b2). Finally, three pulses result in the region bounded by the curve h^3, as is illustrated in Fig. 6.6 (c1)–(c2). Indeed, it is possible to find n-pulse excitability for any n, but the regions for $n > 4$ become impractically small.

It is important to note a key ingredient for multi-pulse excitability to occur, namely the fact that the respective curve h^n extends all the way below ns. For the parameters above ns the h^n-tongues are so narrow that they become hard to distinguish, even numerically. Furthermore, there exist an infinite number of unstable periodic orbits in the phase space for parameters outside the tongues. As a result, the excitable response is often irregular and unpredictable as the trajectory bounces between the unstable orbits before it decides to return to the stable equilibrium. On the other hand, below ns the tongues are easily distinguishable and the phase portraits are simpler as there are no unstable periodic orbits. Consequently, the system can be prepared to be well within h^n (certainly for $n \leq 3$) where the excitable response is predictable and consist of a certain number of pulses.

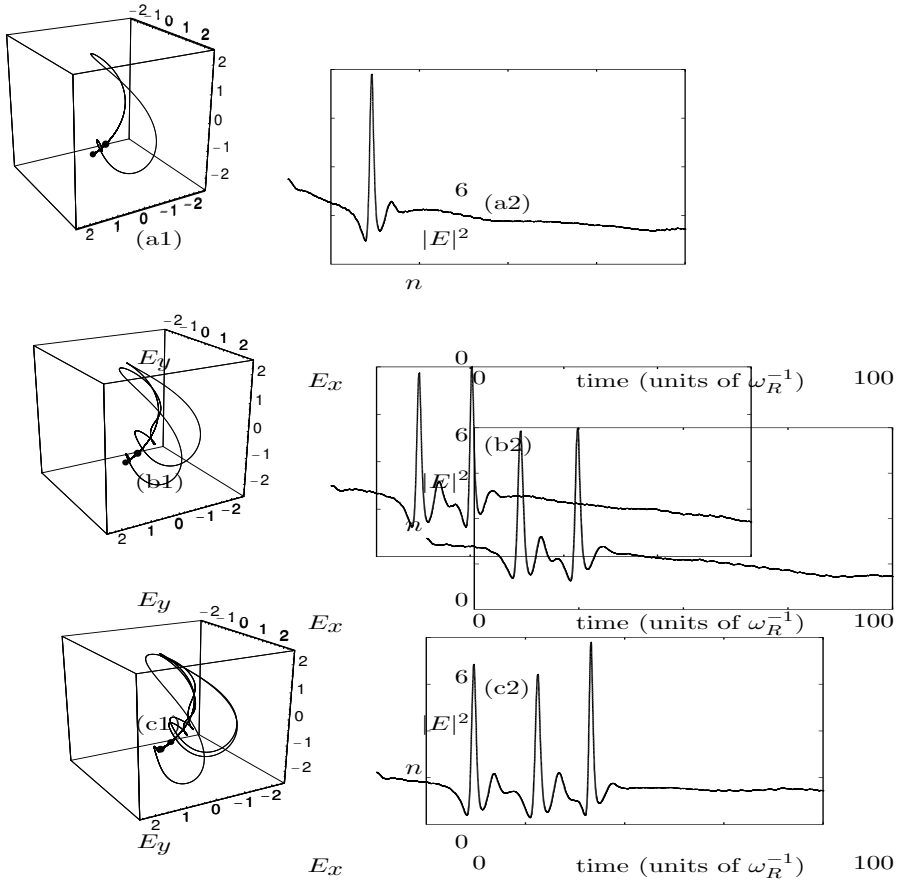

Fig. 6.6. Examples of multi-pulse excitability. The left column shows the phase portrait and the right column the reaction of the laser to a small perturbation above the excitability thresholds. Throughout $\alpha = 1.0$ and from (a) to (c) (K,ω) takes the values $(0.71, -0.95)$, $(0.745. - 1)$ and $(0.735, -0.993)$. From S. Wieczorek and B. Krauskopf, Bifurcations of n-homoclinic orbits in optically injected lasers, *Nonlinearity* 18(3) (2005) 1095–1120 © 2005 by Institute of Physics Publishing; reprinted with permission.

6.1.5 Codimension-Two Homoclinic Bifurcations

We now study in considerable detail the structure and bifurcations associated with the curve h^1 that forms the boundary of the homoclinic teeth. In particular, we show that codimension-two double-homoclinic and T-point bifurcations play a prominent role in organizing the dynamics.

Figure 6.7 shows an enlargement near the first homoclinic tooth (or what is left of it) for $\alpha = 4.5$; compare with Fig. 6.3. Notice the two points D_1 and D_2 where additional homoclinic bifurcation curves emerge. The phase

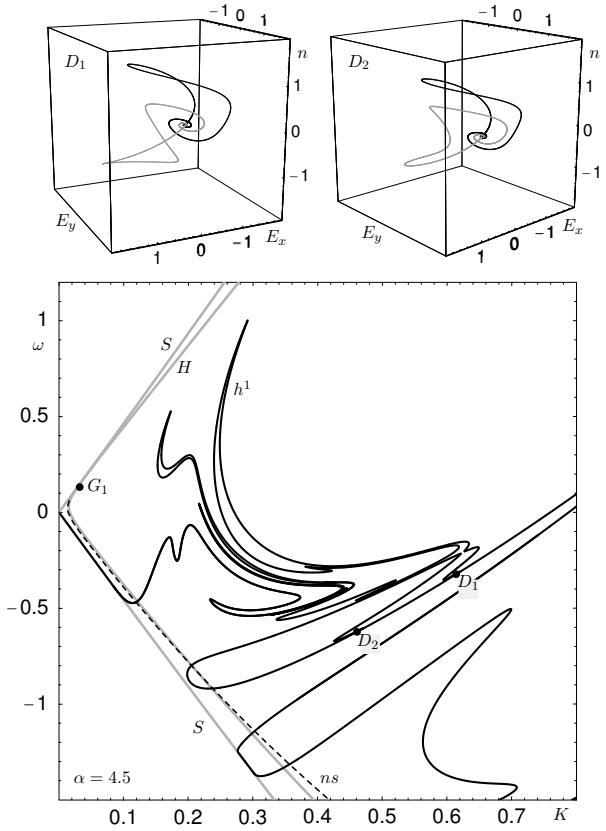

Fig. 6.7. The (K, ω)-plane for $\alpha = 4.5$ near the point G_1 (compare with Fig. 6.3) and the phase portraits at the codimension-two double-homoclinic bifurcation points D_1 and D_2. From S. Wieczorek and B. Krauskopf, Bifurcations of n-homoclinic orbits in optically injected lasers, *Nonlinearity* 18(3) (2005) 1095–1120 © 2005 by Institute of Physics Publishing; reprinted with permission.

portrait at D_1 and D_2 show that we are dealing with a codimension-two *double-homoclinic orbit* [9, 40]: both branches of the unstable manifold spiral back to the saddle point. This means that there are simultaneously two individual homoclinic orbits associated with the same saddle point.

The two phase portraits at D_1 and D_2 are topologically equivalent and both lie on the primary branch of the curve h^1. This can be seen in the further enlargement of the (K, ω)-plane in Fig. 6.8, where panels (a)-(e) show the 1-homoclinic orbit in phase space at the indicated parameter points along h^1. As D_2 is approached the unstable manifold forming a homoclinic orbit comes closer and closer (from below) to the saddle and then leaves a neighborhood of the saddle roughly along the other branch of the unstable manifold. Finally, at D_2 there are two simultaneous homoclinic orbits, one for each branch of the

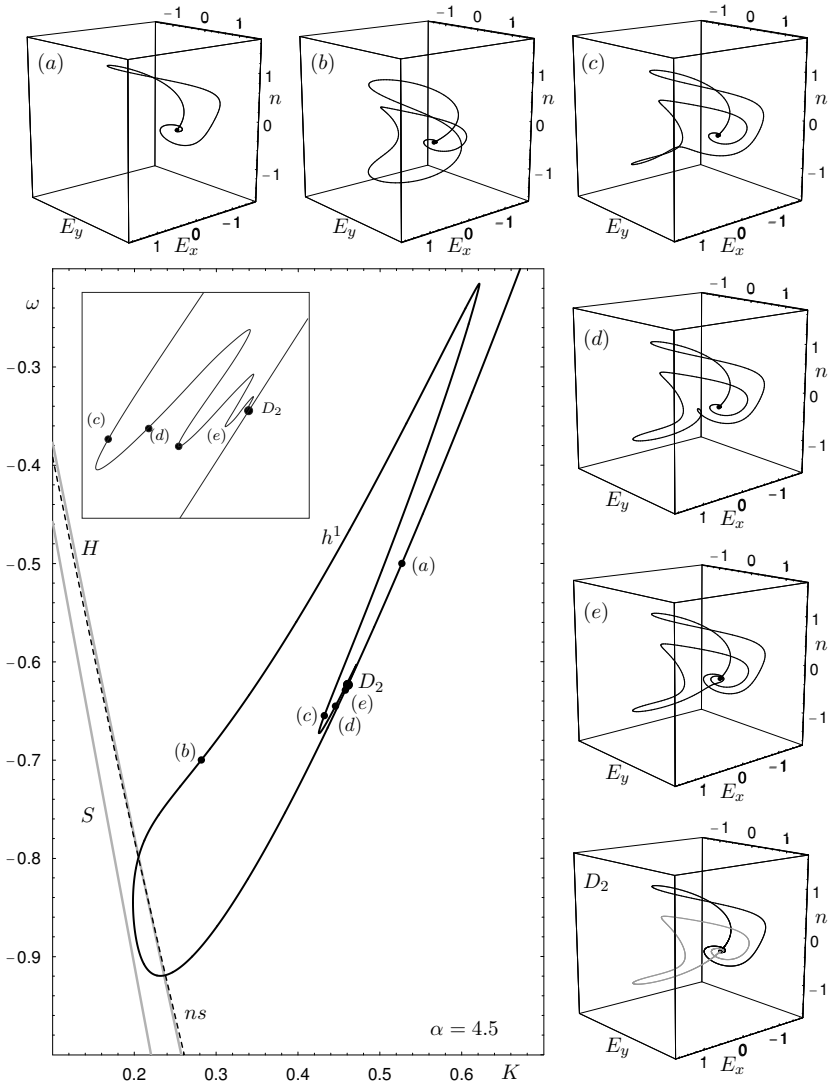

Fig. 6.8. The (K, ω)-plane for $\alpha = 4.5$ near the point D_2 (compare with Fig. 6.7) and the phase portraits along the homoclinic curve h^1 as D_2 is approached. From S. Wieczorek and B. Krauskopf, Bifurcations of n-homoclinic orbits in optically injected lasers, *Nonlinearity* 18(3) (2005) 1095–1120 © 2005 by Institute of Physics Publishing; reprinted with permission.

unstable manifold. Effectively, the original 1-homoclinic orbit along the curves h^1 has split into two homoclinic orbits. Notice that the curve h^1 accumulates back on itself at D_2, as is also sketched in the inset of Fig. 6.8.

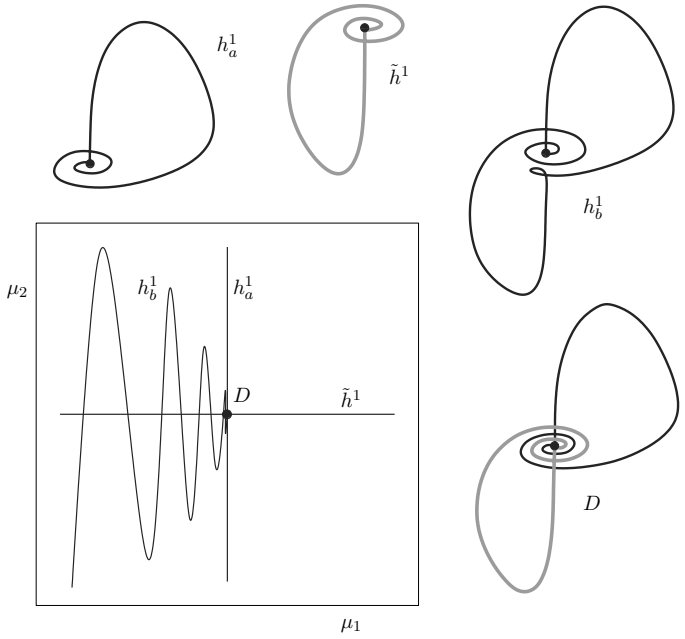

Fig. 6.9. Sketch of phase portraits and the bifurcation diagram (in two unfolding parameters μ_1 and μ_2) of a double-homoclinic point D, as described in [9, 40]. From S. Wieczorek and B. Krauskopf, Bifurcations of n-homoclinic orbits in optically injected lasers, *Nonlinearity* 18(3) (2005) 1095–1120 © 2005 by Institute of Physics Publishing; reprinted with permission.

This scenario agrees with what is known in the literature about the double-homoclinic bifurcation [9, 40]. Again, not all details of this codimension-three global bifurcation are known, but key features are as sketched in Fig. 6.9 (for the case of a saddle focus as we encounter it here). The double-homoclinic orbit D exists at the intersection point of two curves h_a^1 and $\tilde{h}^1$ of two different homoclinic orbits to the same saddle that contain each a different branch of the unstable manifold of the saddle. As sketched, there is a third curve h_b^1 of homoclinic orbits that accumulates on the curve h_a^1. The accumulation is as shown when the saddle quantity is larger than one [9, 40], which is the case we encounter, because all double-homoclinic orbits occur above the curve ns.

Note that the analysis in the literature is in terms of a small tubular neighborhood around the double-homoclinic orbits as sketched in panel D. In this neighborhood the curves h_a^1 and h_b^1 are unrelated. However, as can be seen in Fig. 6.8, they may be one and the same curve accumulating back on itself. In fact, we find this to be the typical situation in system (6.1). We finally stress that the points D_i that we encounter here are of codimension-two because the two simultaneous homoclinic orbits are not related by symmetry. Unlike in the case of a codimension-one symmetric double-homoclinic orbit, it

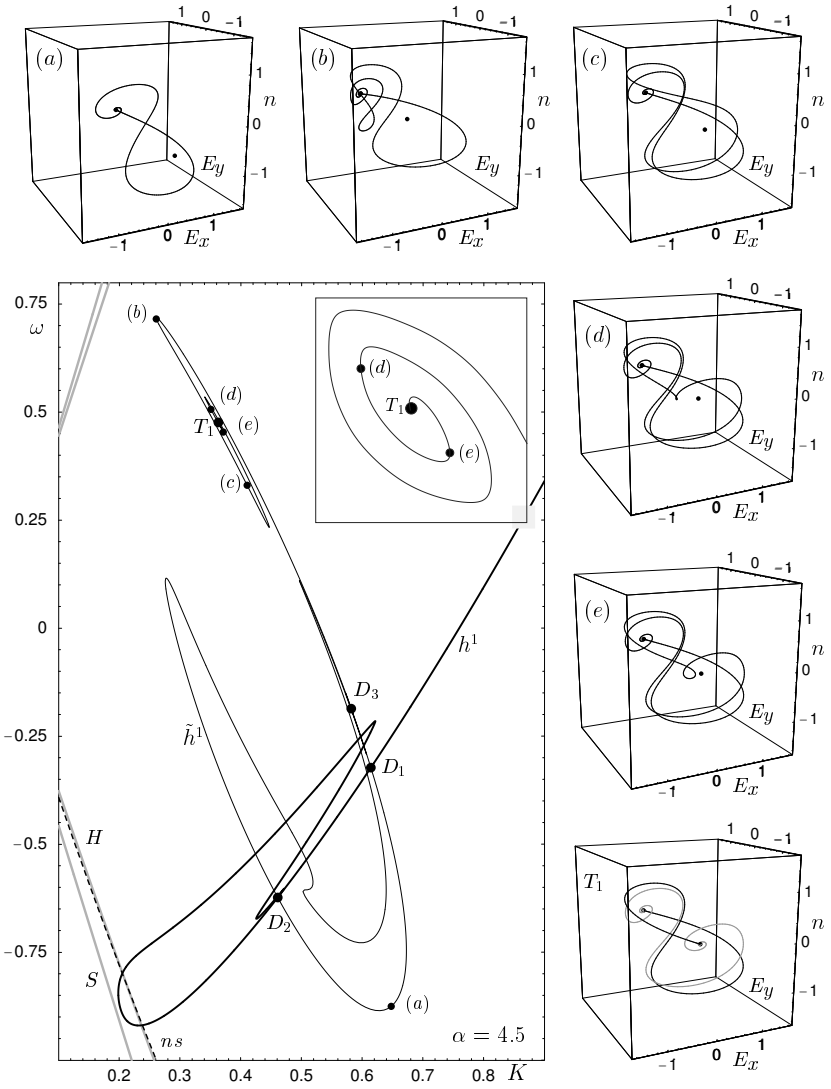

Fig. 6.10. The (K, ω)-plane for $\alpha = 4.5$ near the points D_1, D_2, D_3, and T_1 with phase portraits as T_1 is approached. From S. Wieczorek and B. Krauskopf, Bifurcations of n-homoclinic orbits in optically injected lasers, *Nonlinearity* 18(3) (2005) 1095–1120 © 2005 by Institute of Physics Publishing; reprinted with permission.

is possible to perturb parameters such that one of the homoclinic connections is broken and the other persists.

In Fig. 6.7 and Fig. 6.8 we found the double-homoclinic points D_1 and D_2 as the end points of the curve h^1 as it accumulates on itself. However, we know from Fig. 6.9 that there must be a curve $\tilde{h}^1$ of a second homoclinic orbit

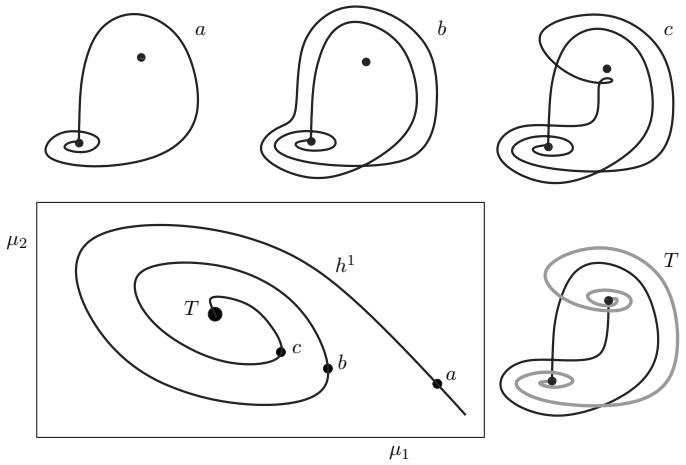

Fig. 6.11. Sketches of the phase portraits along the homoclinic bifurcation curve approaching a T-point in the plane of two unfolding parameters μ_1 and μ_2. From S. Wieczorek and B. Krauskopf, Bifurcations of n-homoclinic orbits in optically injected lasers, *Nonlinearity* 18(3) (2005) 1095–1120 © 2005 by Institute of Physics Publishing; reprinted with permission.

crossing at D_i. In order to find this new homoclinic orbit we split off the new homoclinic orbit from the data of the approximate double-homoclinic orbit at D_i (given as the end point of the curve h^1). We then follow this second codimension-one homoclinic orbit in the (K, ω)-plane.

The result is shown in Fig. 6.10. The point D_2 is indeed the intersection point of two curves of codimension-one homoclinic orbits. The new curve $\tilde{h}^1$ also contains D_1 and has two end points. One end point is a point D_3 of a double-homoclinic orbit, which lies on the curve $\tilde{h}^1$ itself. The other end point is a point denoted by T_1 that is reached in a spiraling fashion, as is also sketched in the inset.

At the point T_1 we encounter a bifurcation that is now generally referred to as a *T-point bifurcation*. This type of codimension-two heteroclinic cycle was studied in a general system, that is, one without any symmetry, in [9, 10] in a tubular neighborhood around the heteroclinic orbits at the T-point. Note that the T-point bifurcation is often associated with vector fields that have the $\mathbb{Z}_2$-symmetry of a rotation by π around an invariant axis. In this case, the heteroclinic cycle involves two saddle-foci, which are each others images under the symmetry, and the origin (more generally, a point in the invariant subspace of the symmetry), which is also a saddle-focus. This $\mathbb{Z}_2$-symmetric T-point bifurcation was initially found and studied in the Lorenz system [22], but also occurs in other systems with rotational symmetry, such as an optically pumped three-level laser [20], an electronic oscillator [19], and a semiconductor

laser with phase-conjugate feedback [26]. It was recently also discovered in systems with the $\mathbb{Z}_2$-symmetry of point-reflection [2, 32]; see also Chap. 7.

What we find is a general T-point bifurcation (that is, in a system without symmetry) for the case that both saddles involved are of saddle foci. The approach to the point T is illustrated in Fig. 6.10(a)–(e) with images of the 1-homoclinic orbit in phase space at the indicated parameter points along the curve $\tilde{h}^1$.

The situation (a part of the bifurcation diagram near a T-point) is sketched in Fig. 6.11. As the point T is approached along h^1, the homoclinic orbit approaches a second saddle focus, passing closer and closer by the saddle. At the point T_1 there are two heteroclinic connections: a codimension-two heteroclinic connection (black) where the one-dimensional unstable manifold of the first saddle coincides with the one-dimensional stable manifold of the second saddle, and a generic (codimension-zero) heteroclinic connection (gray), given as the intersection curve of the two-dimensional stable manifold of the first saddle and the two-dimensional stable manifold of the second saddle.

According to general theory [9, 10] there must exist a second spiraling curve of homoclinic connection to the other (lower) saddle, leading to another curve in parameter space that spirals into T_1. Furthermore, it is known that there are many more curves of n-homoclinic bifurcations, which pass close to the saddles an arbitrary number of times. We did not attempt to find all these bifurcation curves, but instead concentrated on the structure of 1-homoclinic bifurcation curves. Nevertheless, the injection laser appears to be a good model in which to study global bifurcations near T-point bifurcations in more detail.

The bifurcation diagram in Fig. 6.10 is still quite incomplete. The curve $\tilde{h}^1$ of homoclinic orbits also accumulates on itself at D_3. So, as we did near the double-homoclinic point D_1, we find and follow the second codimension-one homoclinic that must exist near D_3. This gives the continuation of the curve h^1 shown in Fig. 6.12, which ends at the point D_1. Furthermore, we followed from near T_1 the codimension-one homoclinic orbit of the (upper) saddle point to lower values of α (see already Fig. 6.13), where we discovered a second T-point bifurcation T_2. We then followed this T-point back to $\alpha = 4.5$. As can be seen in Fig. 6.12, the point T_2 is the end point of two spirals. In fact both spirals turn out to belong to one and the same closed curve of codimension-one two-homoclinic orbit $\tilde{h}^2$ as is illustrated by the sketch in the inset.

The bifurcation diagram in Fig. 6.12 is quite intricate: it involves several double-homoclinic and T-point bifurcations. Unraveling it required detailed numerical continuation with HomCont, guided by theoretical knowledge of which homoclinic orbits are possible near the different codimension-two points. We finally remark, that Fig. 6.12 shows a 'skeleton' consisting of curves of 1-homoclinic bifurcations. Indeed the existence of the T-points suggests that there are n-homoclinic orbits for arbitrary n.

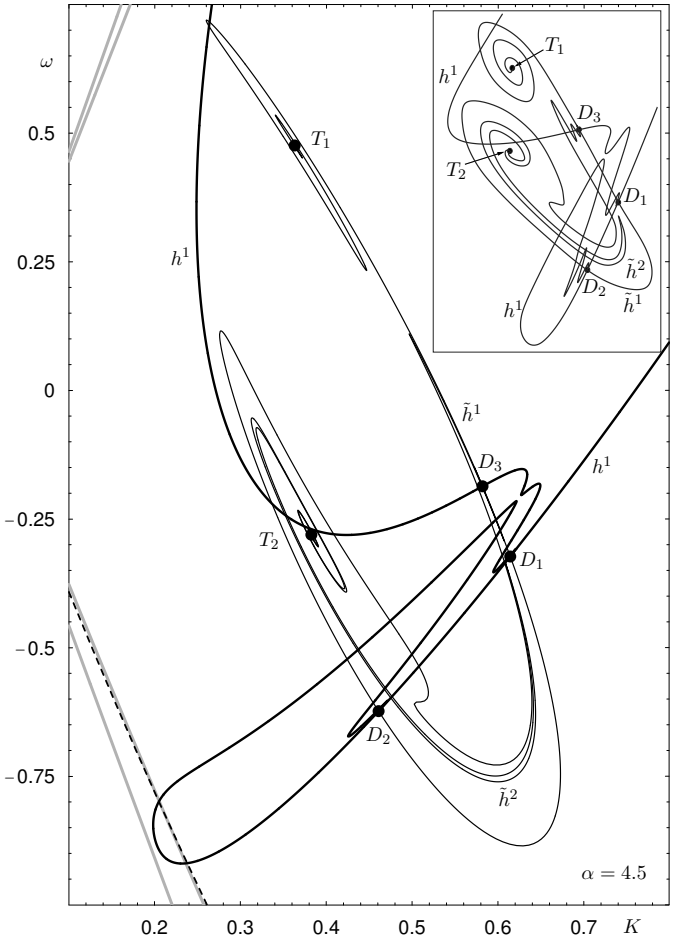

Fig. 6.12. The (K, ω)-plane for $\alpha = 4.5$ near the points T_1 and T_2. From S. Wieczorek and B. Krauskopf, Bifurcations of n-homoclinic orbits in optically injected lasers, *Nonlinearity* 18(3) (2005) 1095–1120 © 2005 by Institute of Physics Publishing; reprinted with permission.

6.1.6 Folds of Codimension-Two Homoclinic Bifurcation Curves

We know from Fig. 6.3 that the complicated structure of codimension-two bifurcations in Fig. 6.12 is not present for smaller values of α. The question arises of how it disappears.

It turns out that an important ingredient in this change of the bifurcation diagram are minima (more generally, a fold) with respect to α of certain curves of codimension-two homoclinic bifurcations in the three-dimensional (K, ω, α)-space. This phenomenon is of codimension three, where one codimension is due to the fold with respect to α. The other two codimensions

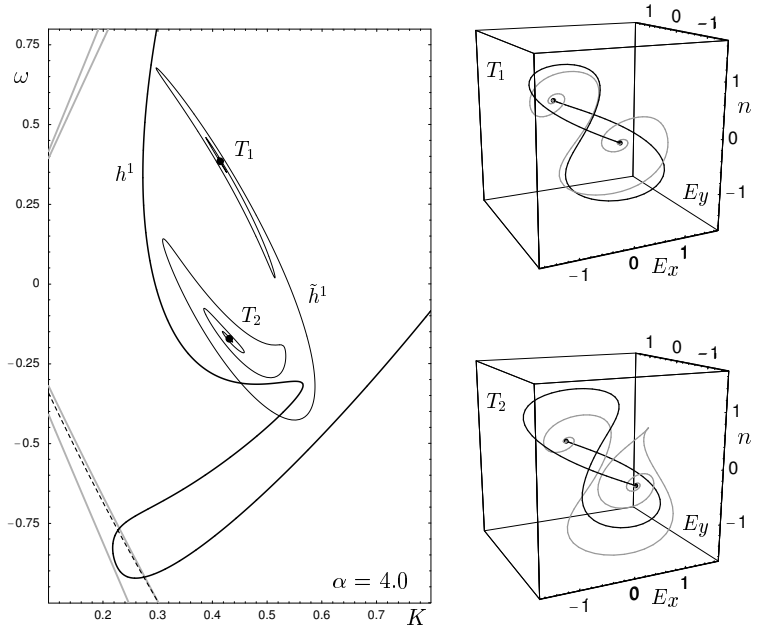

Fig. 6.13. The (K, ω)-plane for $\alpha = 4.0$ near the points T_1 and T_2 and the respective phase portraits at T_1 and T_2. From S. Wieczorek and B. Krauskopf, Bifurcations of n-homoclinic orbits in optically injected lasers, *Nonlinearity* 18(3) (2005) 1095–1120 © 2005 by Institute of Physics Publishing; reprinted with permission.

are due to the special object in phase space, in this case a codimension-two homoclinic bifurcation. One might speak of a codimension-two-plus-one event to distinguish it from codimension-three bifurcations, where all codimensions are due to a codimension-three object in phase space.

We already encountered this phenomenon in the creation and disappearance of points of codimension-two saddle-node homoclinic bifurcation (see the folds with respect to α in Fig. 6.4) and in the creation, with increasing α, of Belyakov points in the tangency between the curves ns and h^1 (see Fig. 6.5). In this section we consider two other examples, namely a fold of a curve of T-point bifurcations and a fold of a curve of double-homoclinic bifurcations. As we will see now, in both these examples the fold of the codimension-two curve is accumulated by singularities in associated surfaces of codimension-one global bifurcations.

We first consider the case of T-point bifurcations. Figure 6.14 shows what happens to the points T_1 and T_2 of T-point bifurcations as α is decreased. After the disappearance of the point D_3, the points T_1 and T_2 move closer and closer to each other. There are a number of codimension-three events where the spiral around T_1 touches that around T_2. Each such event leads to a new closed curve surrounding both T_1 and T_2 and the curve of homoclinic orbits connecting T_1

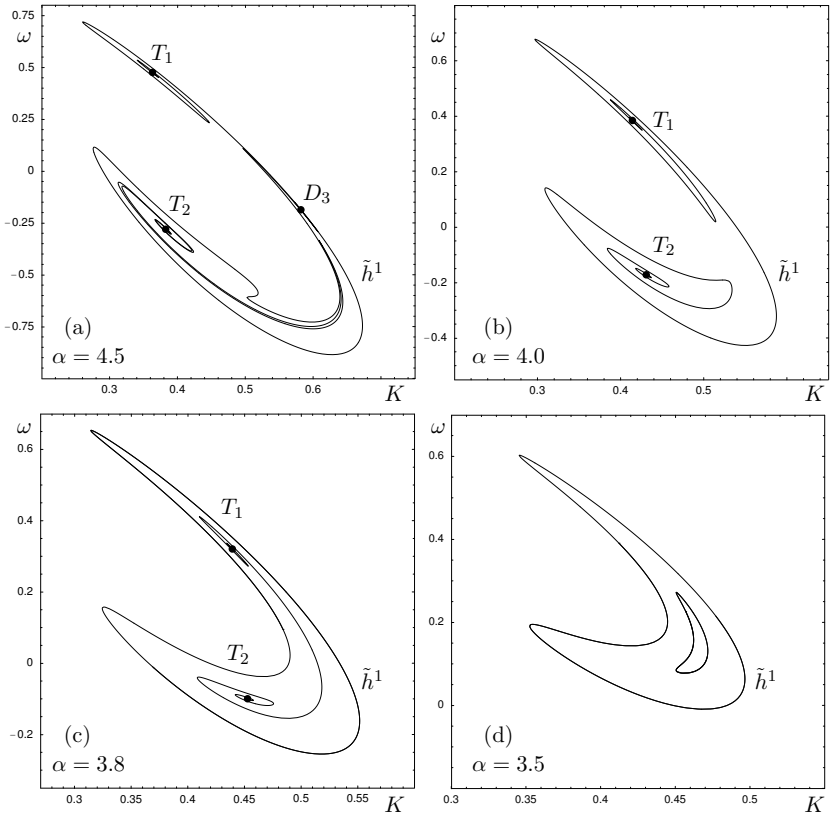

Fig. 6.14. Dependence on α of the (K, ω)-plane near the points T_1 and T_1. From S. Wieczorek and B. Krauskopf, Bifurcations of n-homoclinic orbits in optically injected lasers, *Nonlinearity* 18(3) (2005) 1095–1120 © 2005 by Institute of Physics Publishing; reprinted with permission.

and T_2, as in Fig. 6.14 (c). This process continues until the points T_1 and T_2 finally coincide, leaving behind a number of closed concentric curves of homoclinic orbits, as in Fig. 6.14 (d). These closed curves then disappear one by one as α is decreased further. (We remark that this phenomenon has been found independently in [2] in the $\mathbb{Z}_2$-symmetric Chua's circuit with a cubic nonlinearity; see also Chap. 7.) Finding this transition numerically was quite a challenge because the curves involved are no longer connected. We succeeded by starting from suitable points and continuing the respective homoclinic orbit in α.

The individual changes in the structure of the curve $\tilde{h}^1$ are due to a classical singularity, namely the passage through an α-degenerate point. At such a point, the tangent space to the $\tilde{h}^1$ surface in (K, ω, α)-space does not have an α-component (the derivative with respect to α is zero). There are two

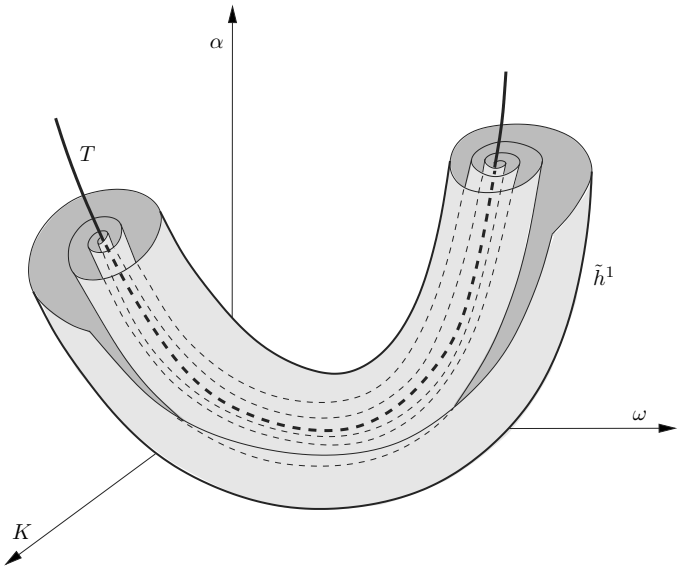

Fig. 6.15. In the (K, ω, α)-space the curve of T-point bifurcation is surrounded by a surface of homoclinic bifurcation $\tilde{h}^1$ that spirals onto the T-curve; compare with Fig. 6.14. From S. Wieczorek and B. Krauskopf, Bifurcations of n-homoclinic orbits in optically injected lasers, *Nonlinearity* 18(3) (2005) 1095–1120 © 2005 by Institute of Physics Publishing; reprinted with permission.

cases depending on the index of the α-degenerate point, namely the transition through a saddle and the transition through an extremum. Note that these singularities are also called the simple bifurcation and the isola bifurcation; see, for example, [23] for details.

This explanation in terms of singularity theory is a consequence of the geometry of bifurcation surfaces and curves in (K, ω, α)-space. In fact, the whole sequence of events of T_1 and T_2 coming together and disappearing can be nicely explained with the sketch in Fig. 6.15 of how the surface $\tilde{h}^1$ of homoclinic bifurcations spirals around the curve T of T-point bifurcations. The curve of T-point bifurcations is a smooth curve with a minimum with respect to α, and it is surrounded by a surface of codimension-one homoclinic bifurcations that spirals towards this curve. The panels in Fig. 6.14 are two-dimensional cross sections for fixed α through this surface. If α is large enough, the curve T is intersected in two points T_1 and T_2 and the spiraling near these two points must be clockwise and counter-clockwise, respectively. The intersection of the surface with the section is a single curve for sufficiently large α. However, nearer the minimum of the curve T the surface has α-degenerate points where its tangent space does not have an α-component. Passing through each such point constitutes a basic codimension-one singularity of the surface of homoclinic bifurcations. More precisely, above the minimum of the curve T

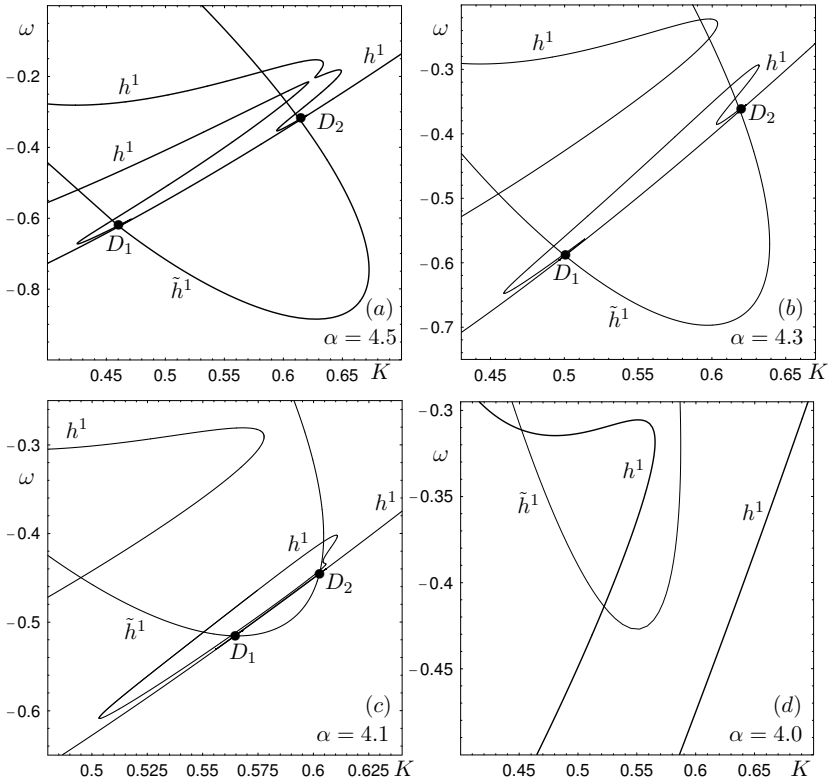

Fig. 6.16. The (K, ω)-plane near D_1 and D_2 for varying α. Points D_1 and D_2 disappear via codimension-three resonant double-homoclinic bifurcation as α is decreased. From S. Wieczorek and B. Krauskopf, Bifurcations of n-homoclinic orbits in optically injected lasers, *Nonlinearity* 18(3) (2005) 1095–1120 © 2005 by Institute of Physics Publishing; reprinted with permission.

there are infinitely many passages through saddles, which accumulate on the minimum of the curve T. Globally, this creates the closed concentric curves by connecting the respective homoclinic curves in a different way. Below the minimum of T, on the other hand, each concentric circle disappears by contracting to a single point, which is the passage through an extremum (with respect to a parameter, in this case α) in a two-dimensional surface $\tilde{h}^1$. We finally remark that it would be quite a challenge to produce a numerical picture of the surface sketched in Fig. 6.15.

Our second example is the merging and disappearance of the points D_1 and D_2 as α is decreased from $\alpha = 4.5$ to $\alpha = 4.0$. Figure 6.16 shows four numerical bifurcation diagrams in this transition. As the points D_1 and D_2 are moving closer together we again encounter a passage through a saddle point. This happens between panels (a) and (b) of Fig. 6.16 and it leads to a

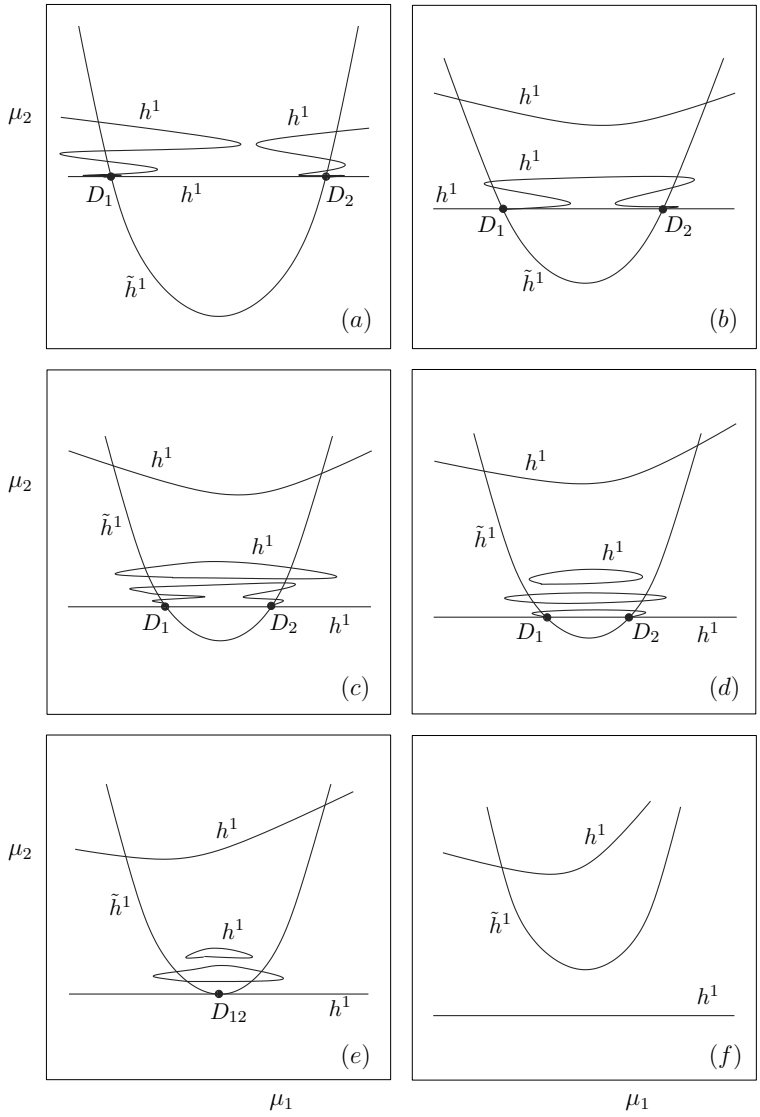

Fig. 6.17. The sketch of how D_1 and D_2 disappear via codimension-three resonant double-homoclinic bifurcation in the two unfolding parameters μ_1 and μ_2. Compare with Fig. 6.16. From S. Wieczorek and B. Krauskopf, Bifurcations of n-homoclinic orbits in optically injected lasers, *Nonlinearity* 18(3) (2005) 1095–1120 © 2005 by Institute of Physics Publishing; reprinted with permission.

change in how the curves h^1 in the cross section in the (K, ω)-plane connect. After this event, the curve h^1 in Fig. 6.16(b) connects the two points D_1 and D_2. In a further passage through a saddle point the curve h^1 pinches

off to create an isola, which is the situation shown in Fig. 6.16(c). In fact, the isola is very close to the new connection between D_1 and D_2. Numerical continuation suggests that more and more isolas are formed as D_1 and D_2 come closer together. These isolas then disappear in passages through minima. Furthermore, α passes through the minimum of the D curve in the (K, ω, α)-space. As a result, the curves $\tilde{h}^1$ and h^1 in Fig. 6.16(d) no longer intersect and the points D_1 and D_2 have disappeared.

To clarify the situation, we sketch the transition leading to the disappearance of D_1 and D_2 in Fig. 6.17. It can again be understood by the geometry of bifurcation surfaces in (K, ω, α)-space, which in this case are organized around a minimum (with respect to α) of the curve D of double-homoclinic bifurcations. Figure 6.17(a)–(c) and (f) are topologically as the numerical bifurcation diagrams in Fig. 6.16(a)–(d), respectively. We remark that it becomes more and more difficult to resolve numerically the different, small and disjoint intersection curves of the surface h^1 in (K, ω, α)-space. The sketches in Fig. 6.17(d) and (e) are based on our numerical investigations, and indicate how the transition appears to take place. However, the exact details, in particular, the order in which isolas are created and shrink to points and disappear is yet unknown. Our continuation study suggests the basic ingredients of this transition and can reveal some of the first steps in the specific transition at hand. This scenario agrees with what is known about the (local) codimension-two bifurcation diagrams near a double-homoclinic bifurcation as sketched in Fig. 6.9, but a complete study of this codimension-two-plus-one phenomenon remains a challenge.

The fact that we encounter minima in curves T and D confirms the experience from simulations and experiments that the dynamics and the bifurcation diagram of the injected laser become more complicated as the line-width enhancement factor α is increased [59]. Indeed, when α is increased past these minima extra organizing centers, T-points or double homoclinic bifurcation points, are born. These events are associated with infinitely many transitions through saddles and extrema in surfaces of global bifurcations. Furthermore, general theory shows that the emerging T-points or double homoclinic bifurcation points are organizing centers that give rise to n-homoclinic orbits for any n.

6.1.7 A Self-Similar Cascade Phenomenon

As a final example of the increase in the complexity with α we show in Fig. 6.18 the bifurcation diagram in the (K, ω)-plane for $\alpha = 6.0$ near the point G_1. Notice that we only show the different parts of the curve h^1 of one-homoclinic orbits, which form what is left from the left most homoclinic tooth near G_1; compare with Fig. 6.3(f). Near the points D_1 and D_2, that were already found for $\alpha = 4.5$, we find two new points D_4 and D_5; compare with Fig. 6.7. The different bifurcation curves are very close together, and the inset shows a topological sketch of the bifurcation diagram. Notice further that two extra

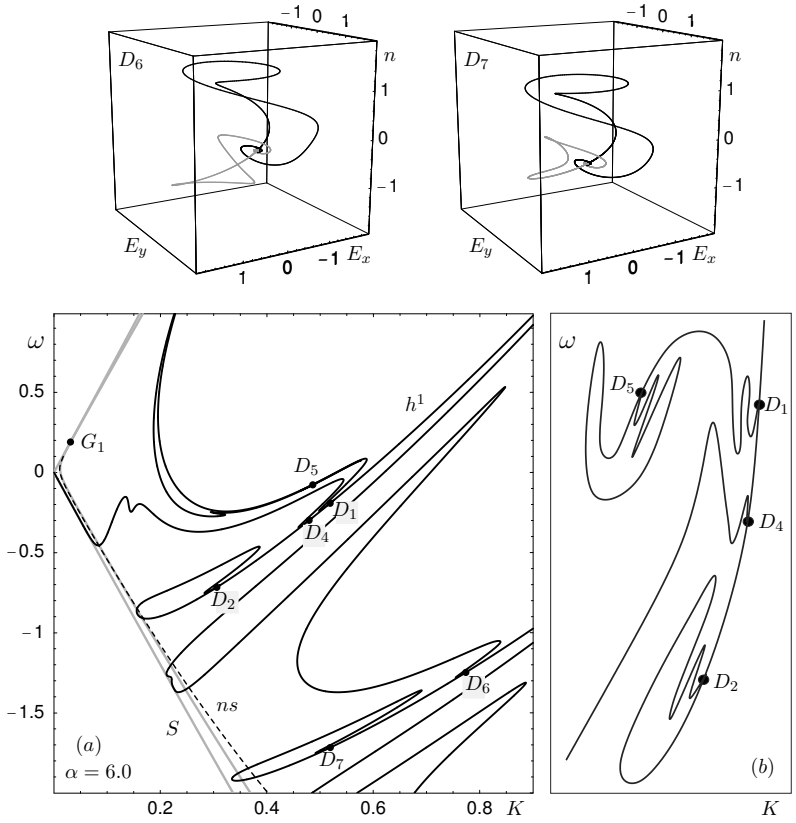

Fig. 6.18. The (K, ω)-plane for $\alpha = 6.0$ near the point G_1 (compare with Fig. 6.3) and the phase portraits at the codimension-two points D_6 and D_6. From S. Wieczorek and B. Krauskopf, Bifurcations of n-homoclinic orbits in optically injected lasers, *Nonlinearity* 18(3) (2005) 1095–1120 © 2005 by Institute of Physics Publishing; reprinted with permission.

double-homoclinic bifurcation points D_6 and D_7 have just been created in the same way as D_1 and D_2 previously. This is another example of the passage through a minimum of a curve D of double-homoclinic orbits; compare with Fig. 6.7.

Figure 6.18 shows that in the injected laser we are dealing with a type of cascade phenomenon: complicated bifurcation scenarios found for one tooth also occur for all the other teeth when α is increased.

6.1.8 Concluding Remarks on Injected Lasers

This section presented a detailed study of the bifurcations of n-homoclinic orbits in the rate equations describing a semiconductor laser with optical in-

jection. The corresponding curves of n-homoclinic bifurcations are organized in what we call homoclinic teeth, experimentally accessible regions inside the locking region of the laser. The analysis of the bifurcation diagram from a global viewpoint proved to provide new insight into the nature of global bifurcations and allowed us to identify a cascade phenomenon where complicated bifurcation scenarios repeat for subsequent homoclinic teeth.

The injection laser rate equations emerged as a concrete vector field in which complicated global bifurcations can be found and studied. Specifically, we found in this three-dimensional vector field (without any additional symmetries) T-point bifurcations and double-homoclinic orbits. By making extensive use of continuation techniques for homoclinic and heteroclinic orbits, it is possible to study these codimension-two global bifurcations themselves, and also to find out how they organize the corresponding bifurcation diagrams.

When changing a third parameter, we found a new phenomenon, namely complicated transitions in two-parameter bifurcation diagrams that are due to folds (in this case, minima) in codimension-two curves of global bifurcations. These 'codimension-two-plus-one events' come with accumulations of singularity transitions through saddles and extrema, which can be explained by the geometry of surfaces of global bifurcations in a three-dimensional parameters space. Our results raise a number of questions of bifurcation theory. In particular, a detailed study of the unfoldings of the 'codimension-two-plus-one events' remains a challenging task.

From the physical point of view, we presented here how the regions in which one may find multi-pulse excitability depend on the linewidth-enhancement factor α. Our results confirm that the dynamics and bifurcations of an injected laser are more complex the larger the linewidth enhancement factor α. Most importantly, they stimulated new laser experiments. The already demonstrated good agreement between theory and experiment on the level of local bifurcations in the injection laser [65, 66] has now been extended to global bifurcations such as the ones described here. In fact, the predicted effect of multi-pulse excitability was recently measured independently by two different groups [8, 25].

6.2 Phase-Locking Anomaly in Two Back-to-Back Coupled Lasers

This section is based on [53, 54] and concerned with the dynamics and bifurcations of two coupled lasers. We model the system with spatial composite-cavity modes that describe the entire coupled-laser structure [13, 43]. This is in contrast to the more usual approach of modeling the individual uncoupled lasers and then introducing the coupling via ad-hoc terms in the equations of motion.

It is generally believed that the transition from weakly-coupled to totally isolated lasers occurs smoothly. This means that, as the coupling approaches

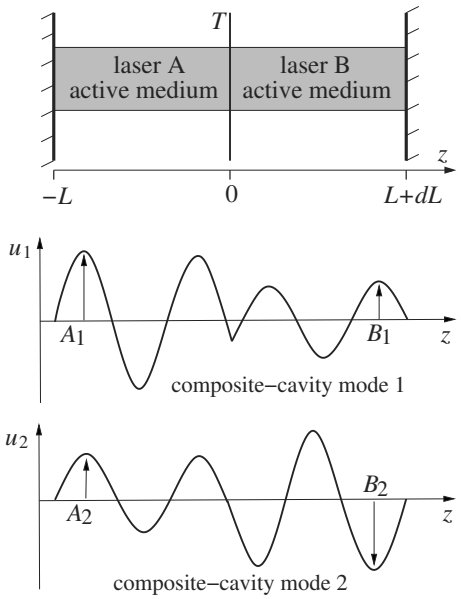

Fig. 6.19. Two back-to-back coupled lasers (top), and a pair of composite-cavity modes (bottom).

zero, there is an uninterrupted vanishing of the detuning range over which phase-locking is achieved. We show here that there is an anomaly in the transition from coupled to totally isolated lasers. Namely, this transition does not occur smoothly but is interrupted with the occurrence of instabilities and even chaotic dynamics. Importantly, there exists an open interval of the coupling strength where phase locking is impossible at any detuning.

To understand these counter-intuitive phenomena we study in detail two-dimensional bifurcation diagrams in the plane of laser detuning and coupling strength for different values of the linewidth enhancement factor α; see Sect. 6.1.1. The analysis reveals various codimension-two bifurcations including saddle-node-Hopf and generalized Hopf bifurcations, 1:1 and 1:2 resonances, and homoclinic-doubling points. In particular, we identify codimension-three bifurcations leading to the appearance of a gap in the phase-locking region with increasing α. Furthermore, we perform a detailed study of bifurcations of periodic orbits, and specifically their origins and mutual connections, to show how the gap is gradually occupied by instabilities and chaos with increasing α.

6.2.1 Composite-Cavity Description of Two Back-to-Back Coupled Lasers

We consider two laser cavities with instantaneous (no time delay) coupling: cavity A of length L is coupled via a common mirror of transmission T to cavity B of length $L + dL$; see Fig. 6.19. For the consistent description of coupling and optical nonlinearities, we expand the spatiotemporal laser field $\mathcal{E}(z,t)$ in terms of standing waves $u_n(z)$ for the *entire* double-cavity cavity structure [13, 43, 53]

$$\mathcal{E}(z,t) = \frac{1}{2}\sum_j \left[E_j(t)e^{-i\Psi_j(t)}u_j(z) + c.c.\right]. \tag{6.2}$$

Such standing waves are called composite-cavity modes. This is in contrast to the usual approach that neglects spatial effects in the coupling. Notice, that in the composite-cavity-mode picture, the resulting equations describe interaction of composite-cavity modes rather than individual lasers [52].

Mathematically, the situation is described by a system of two globally coupled oscillators that can be described by the set of five autonomous ordinary differential equations

$$\begin{aligned}\dot{E}_j = -\gamma E_j + C_{jj}\gamma \times \sum_{k=1,2} \Big\{ &[C_{kj}^A(1+\beta N_A) + C_{kj}^B(1+\beta N_B)]\cos(\psi_{kj}) \\ &-\alpha\beta[C_{kj}^A(1+N_A) + C_{kj}^B(1+N_B)]\sin(\psi_{kj})\Big\} E_k,\end{aligned} \tag{6.3}$$

$$\begin{aligned}\dot{\Psi}_j = \Omega_j + C_{jj}\gamma \times \sum_{k=1,2} \Big\{ &\alpha\beta[C_{kj}^A(1+N_A) + C_{kj}^B(1+N_B)]\cos(\psi_{kj}) \\ &+[C_{kj}^A(1+\beta N_A) + C_{kj}^B(1+\beta N_B)]\sin(\psi_{kj})\Big\}\frac{E_k}{E_j},\end{aligned} \tag{6.4}$$

$$\dot{N}_{A/B} = \Lambda - (N_{A/B}+1) - \sum_{k,j=1,2} C_{kj}^{A/B}\,(1+\beta N^{A/B})\cos(\psi_{kj})\,E_kE_j, \tag{6.5}$$

where $j = 1,2$ and $\psi_{kj} = \Psi_k - \Psi_j$ is the phase difference between mode k and mode j. (Note that it is sufficient to consider the equation for the phase difference ψ_{12} between the two electric fields.) Equations (6.4)–(6.5) are coupled to the algebraic constraints

$$\sin\left[\frac{\Omega_j}{c}n_b(2L+dL)\right] = 2\frac{\sqrt{1-T}}{T}\sin\left[\frac{\Omega_j}{c}n_bL\right]\sin\left[\frac{\Omega_j}{c}n_b(L+dL)\right], \tag{6.6}$$

$$\begin{aligned}A_j^2L\left[\frac{1}{2} - \frac{\sin\left(2\frac{\Omega_j}{c}n_bL\right)}{4\frac{\Omega_j}{c}n_bL}\right] + B_j^2(L+dL)\left[\frac{1}{2} - \frac{\sin\left[2\frac{\Omega_j}{c}n_b(L+dL)\right]}{4\frac{\Omega_j}{c}n_b(L+dL)}\right] \\ +A_j^2\frac{2c}{\Omega_jn_b}\frac{\sqrt{1-T}}{T}\sin^2\left(\frac{\Omega_j}{c}n_bL\right) = L,\end{aligned} \tag{6.7}$$

$$A_j \sin\left(\frac{\Omega_j}{c} n_b L\right) = -B_j \sin\left[\frac{\Omega_j}{c} n_b (L + dL)\right], \tag{6.8}$$

$$C_{jk}^{A}(T, dL) = \frac{1}{L}\int_{-L}^{0} dz u_j(z) u_k(z), \tag{6.9}$$

$$C_{jk}^{B}(T, dL) = \frac{1}{L}\int_{0}^{L+dL} dz u_j(z) u_k(z). \tag{6.10}$$

Differential equations (6.3)–(6.5) describe the time evolution of the real field amplitudes E_1 and E_2 of the composite-cavity modes, their phase difference ψ_{12}, and the population inversion in lasers A (N_A) and B (N_B). The modal frequencies Ω_1 and Ω_2 are determined from the transcendental equation (6.6), the modal amplitudes $A_{1/2}$ and $B_{1/2}$ are determined from (6.7)–(6.8), and the coupling coefficients C_{jk}^{A} and C_{jk}^{B} are determined from the spatial overlap of the composite-cavity modes; see (6.9)–(6.10). More details on the derivation of the model, algebraic constraints, and dimensionless parameters can be found in [13, 52, 53].

The aim is to calculate two-dimensional bifurcation diagrams of system (6.3)–(6.5) in the (T, dL)-plane for different fixed values of the linewidth enhancement factor α. For the other parameters we chose the realistic values, namely for the refractive index $n_b = 3.4$, for the dimensionless gain coefficient $\beta = 9.82$, for the dimensionless excitation rate $\Lambda = 2$ in cavity A and B, and for the ratio of the composite-cavity and population decay rates $\gamma = 10$. Because of the nature of the model, the bifurcation analysis of the coupled-laser system is not as straightforward as in the case of the optically injected laser in Sect. 6.1. The two main issues are:

1. the coupling parameters (which are the main bifurcation parameters) namely, the coupling-mirror transmission T and the cavity-length mismatch dL, appear in (6.3)–(6.5) implicitly through the modal frequencies Ω_1 and Ω_2 and integrals C_{jk}^{A} and C_{jk}^{B} as described by (6.6)–(6.10);
2. the system has two types of periodic solutions: those where the phase difference ψ_{12} is bounded within a 2π interval, and those where ψ_{12} is unbounded, that is, $\psi_{12}(t)$ is periodic modulo 2π; the latter oscillations are also called rotations [16].

The first issue can be overcome by appending the algebraic constraints (6.6)–(6.10) to the system of ODEs (6.3)–(6.5) and solving the extended system, that is, by performing continuation of solutions to (6.3)–(6.5) and (6.6)–(6.10) simultaneously. The second issue becomes problematic only near transitions between periodic solutions with bounded and unbounded phase. (Each individual type of periodic solution is readily continued with AUTO.) Such transitions are common near interesting phenomena (e.g., codimension-two saddle-node-Hopf points with re-injection) and may cause technical inconvenience. This issue can be overcome in the case of two laser modes by appropriate

change of variables [46]. However, it remains an interesting issue for the bifurcation analysis of multi-mode lasers where phase relations between more than two individual modes need to be taken into account.

6.2.2 Symmetry Properties

It is interesting to discuss symmetries in the presence of two composite-cavity modes. Because each composite mode has different spatial overlap with the active media there is no perfect symmetry in the system of coupled-cavity lasers. However, for long (compared to the wavelength $\lambda = 1\mu$m) cavities this difference is small enough so that the system appears to have some symmetries. If $L \gg \lambda$ (this works well already when $L \sim 10\lambda$), we have that $C^A_{jj} \simeq C^B_{kk}$, and $C^A_{jk} \simeq -C^B_{jk}$ for $j \neq k$. Furthermore, if $L \gg \lambda$ and $dL \sim \lambda$ we have that the symmetry $(C^A_{jj}, dL) \to (C^B_{jj}, -dL)$. One consequence of the above relations is the (approximate) reflection symmetry $(\psi_{kj}, N^A, N^B, \alpha, \Lambda, dL) \to (\psi_{kj} \pm \pi, N^B, N^A, \alpha, \Lambda, -dL)$. Hence, the bifurcation diagram in the (T, dL) plane can be symmetric with respect to the change $dL \to -dL$, provided that both lasers have equal excitation rates Λ and equal linewidth enhancement factors α.

Another consequence is the symmetry in the phase space. Under the assumption of equally pumped lasers, equal losses for both composite-modes, and zero linewidth enhancement factor $\alpha = 0$, if $\{E^0_1, E^0_2, \psi^0_{12}, N^0_A, N^0_B\}$ is an equilibrium, then we notice that $\{E^0_1, E^0_2, \psi^0_{12} \pm \pi, N^0_B, N^0_A\}$ is an equilibrium too. Each of the two points may sometimes be associated with lasing at a single composite-cavity mode. Whether both of them are stable at the same time depends on the competition between the composite-cavity modes. Strong competition results in bistability between these two equilibria [42].

6.2.3 Chaos in Practically Isolated Microcavity Lasers

In recent studies focusing on coupled lasers little attention has been devoted to dynamical properties of practically uncoupled lasers, although such lasers are encountered in a wide range of applications. By practically uncoupled or isolated lasers, we mean two or more lasers where the desire is for the lasers to operate totally independent of one another, while in practice, only partial isolation is possible. Practically isolated lasers are encountered in the modern technology of micro-optical circuits, where one faces the problem of reducing cross-talk between laser diodes that are densely integrated onto a single chip.

Figure 6.20 depicts the bifurcation diagram in the (T, dL)-plane for two microcavities described by (6.3)–(6.5) with $L = 2.8\mu$m and $\alpha = 2$, where supercritical bifurcations are plotted as solid curves, and subcritical bifurcations as dashed curves. Phase-locking of lasers corresponds to the situation where both lasers emit light of constant intensities and the same frequency. This can be achieved in two ways: through phase locking of the composite-cavity

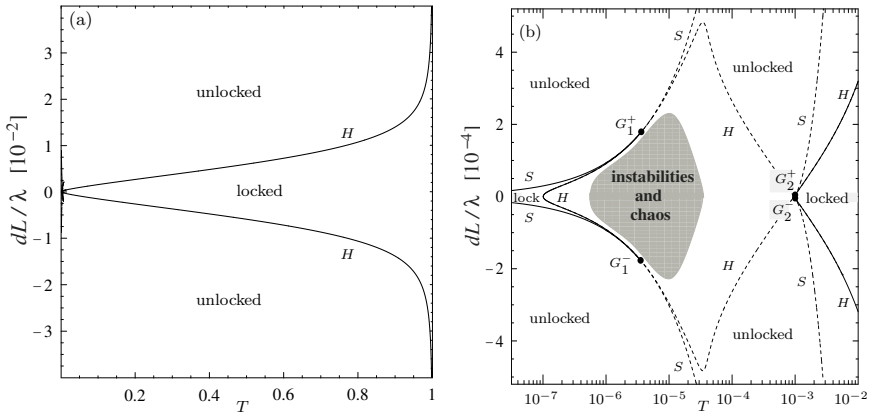

Fig. 6.20. Bifurcation diagram of (6.3)–(6.5) in the $(T, dL/\lambda)$-plane of coupled microcavity lasers (a), and an enlargement for very small T (b). From S. Wieczorek and W.W. Chow, Chaos in practically-isolated microcavity lasers, *Phys. Rev. Lett.* 92 (2004) 213901 © 2004 by the American Physical Society; reprinted with permission.

modes or when both lasers operate at a single composite-cavity mode. In the $\{E_1, E_2, \psi_{12}, N_A, N_B\}$ phase space, phase locking is represented by an equilibrium. The phase-locking region in Fig. 6.20(a), where the lasers operate with a single composite-cavity mode, is indicated by the region between the two supercritical branches of Hopf bifurcation curve H. The locked state is lost when H is crossed towards higher values of $|dL|$. No other transition is visible at this scale and the general features at moderate coupling are similar to what is generally expected. The transition from weakly-coupled to totally isolated lasers appears to occur smoothly, i.e., with an uninterrupted vanishing of the phase locking region, as the coupling approaches zero.

However, the coupled-laser behavior contains an anomaly, whose presence is only noticeable with significant magnification of the (T, dL) parameter space in the vicinity of the origin as shown in Fig. 6.20(b). There, we find the curves of saddle-node and Hopf bifurcation, S and H, respectively. These curves are tangent at four codimension-two saddle-node-Hopf points where they change from sub- to super-critical. These saddle-node-Hopf points are often origins of complex bifurcation structures that give rise to chaos [33]. Starting from the right, the phase-locking region closes near G_2^+ and G_2^- where the two branches of S merge. Phase-locking reappears at G_1^+ and G_1^- and ends at the origin of the (T, dL)-plane. In the notation of [33] G_1 and G_2 belong to different types of saddle-node-Hopf points. Both types are associated with a complex web of bifurcations roughly indicated by the shaded region in Fig. 6.20(b) and studied in more detail in the next section. As the coupling approaches zero, one expects the oscillators to be more independent. Instead, they start interacting in a most complicated way and exhibit mutually induced chaotic

oscillations. An interesting question arises as to the origin of this intriguing and counter-intuitive example of coupled nonlinear-oscillator behavior.

6.2.4 Origin of the Interrupted Phase-Locking Region

To explore the dependence of the coupled-laser instabilities on the resonator length L, and to avoid technical difficulties associated with continuation of bifurcation curves across eight orders of magnitude in T (see Fig. 6.20) we now consider longer laser cavities with $L = 280\mu$m.

Bifurcations of Equilibria for $\alpha = 0$

The case of $\alpha = 0$ is highly degenerate and has an uninterrupted phase-locking range as is shown in Fig. 6.21. The two composite-cavity modes are in strong competition leading to bistable locking range. Saddle-node and Hopf bifurcations associated with both stationary points are tangent at $T \approx 0.027$, at four codimension-two saddle-node-Hopf points. Starting inside the locking range and increasing $|dL|$, the locking is lost either via saddle-node bifurcation ($T < 0.027$) or via Hopf bifurcation ($T > 0.027$). Although there are two different bifurcations responsible for the locking-unlocking transition, one can distinguish three different locking-unlocking mechanisms.

For $T < 0.027$ each of the two bifurcating stable equilibria has contributions from both composite modes; see Fig. 6.21(a). Here, frequency separation of the two composite-cavity modes is small, and the laser locking-unlocking transition is a transition between two composite-cavity modes which are phase-locked and two composite-cavity modes which are phase-unlocked. Locking of the lasers arises from phase-locking of the composite-cavity modes. In the $\{E_1, E_2, \psi_{12}, N_A, N_B\}$ space this is represented by two (there is bistability) saddle-node bifurcations of equilibria that take place on a single periodic orbit. Unlocked operation is represented by a single stable periodic orbit.

For $T > 0.15$, each of the two bifurcating stable equilibria has a large contribution from one composite mode, and a vanishing contribution from the other composite mode. The laser locking-unlocking transition is a transition between a single composite-cavity mode (see Fig. 6.21(a)) and two phase-unlocked composite-cavity modes. Locking of the lasers arises from strong competition (owing to strong cross-saturation) between the two composite modes [13, 52]. In the $\{E_1, E_2, \psi_{12}, N_A, N_B\}$ space, this is represented by two supercritical Hopf bifurcations leading to two stable periodic orbits. It also involves saddle-node bifurcation of periodic orbits in which one of these stable orbits disappears. Consequently, unlocked operation is represented by a single stable periodic orbit [53] and no instabilities appear with increasing $|dL|$.

The most interesting region lies in between the two, near the points $G_j^{\pm}$, where neither the composite-mode phase-locking nor the competing

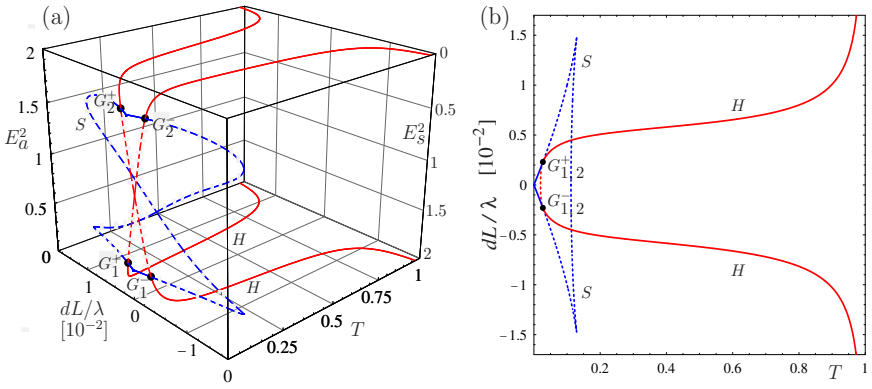

Fig. 6.21. Bifurcations of equilibria of (6.3)–(6.5), shown as a three-dimensional bifurcation diagram in the $(T, dL/\lambda, E^2_{1/2})$-space (a), and as a projection onto the $(T, dL/\lambda)$-plane (b). The supercritical parts (darker solid curves) of the saddle-node bifurcation curve S (blue) and the Hopf bifurcation curve H (red) bound the phase-locking region. S and H are tangent and change from super- to subcritical at codimension-two saddle-node-Hopf points $G_j^{\pm}$. From S. Wieczorek and W.W. Chow, Global view of nonlinear dynamics in coupled-cavity lasers-a bifurcation study, *Opt. Comm.*, 246(4–6) (2005) 471–493 © 2004 by Elsevier Science; reprinted with permission.

composite-cavity-mode description is valid. This is where the beat note frequency $\dot{\psi}_{12}$ comes close to the laser's characteristic relaxation oscillation frequency, which is known to give rise to nonlinear resonances and chaos. For $0.027 < T < 0.1$, starting within the phase-locking region, locking of the lasers is lost via undamping of the relaxation oscillation at a Hopf bifurcation. The two stable stationary points become unstable and each of them gives rise to one stable periodic orbit. Outside the phase-locking region and near $G_j^{\pm}$, these two periodic orbits (bistability in unlocked operation) encounter instabilities leading to complicated dynamics and chaos. It is interesting to note that, as T increases, the transition between the first and the second locking mechanism is clear cut, indicated by $G_j^{\pm}$. On the other hand, the transition between the second and the third locking mechanism happens continuously and involves saddle-node bifurcation of periodic-orbits.

As a result of the degeneracy of the case $\alpha = 0$, in the projection of the bifurcation diagram onto the $(T, dL/\lambda)$ plane shown in Fig. 6.21(b) bifurcations of different stationary states appear as a single curve or point. How can this degeneracy be removed?

Influence of α on Bifurcations of Equilibria

To explore the dynamics of different types of lasers and to understand how qualitative differences in the behavior of different lasers come about, we focus

our attention on the evolution of the phase-locking region with increasing α. The two phase-locking regions in Fig. 6.22, associated with the two stable equilibria, are distinguished by left-inclined and right-inclined patterning, respectively. Let us recall that bifurcation theory predicts four different types of saddle-node Hopf points. All four points $G_j^{\pm}$ from Fig. 6.22(a) are of type IV in the notation from [33].

Increasing α above zero unfolds the otherwise degenerate bifurcation diagram in Fig. 6.22(a) so that for nonzero α neither bifurcation curves nor $G_1^{\pm}$ and $G_2^{\pm}$ fully overlap any longer [Fig. 6.22(b)]. One phase-locking region, associated with G_1^+ and G_1^-, expands along the dL/λ axis and moves in the direction of lower values of T. The other phase-locking region, associated with G_2^+ and G_2^-, moves together with G_2^+ and G_2^- in the direction of higher values of T. Furthermore, the phase-locking region associated with G_1^+ and G_1^- is no longer bounded by the entirely supercritical Hopf bifurcation curve. Codimension-two generalized-Hopf bifurcation points H_g appear where the Hopf curve changes from supercritical to subcritical. Throughout the range of α under consideration, the type of G_2^+ and G_2^- remains unchanged. On the other hand, G_1^+ and G_1^- change from type IV to type III (in the notation from [33]) at $\alpha \simeq 0.5$. The bifurcation diagram in Fig. 6.22(c) shows that the curve H has a cusp at G_1^+ and G_1^- which makes this a very special point, namely a bifurcation of codimension at least three. During the change in the type of G_1^+ and G_1^- the two associated branches of H, one supercritical and the other subcritical, locally exchange their order. This has important consequences to where the chaotic dynamics associated with $G_1^{\pm}$ appear; see the next subsection for explanation. Increasing α further results in less overlap between the two phase-locking regions to the point where they no longer coalesce [Fig. 6.22(d)]. At $\alpha = 1$ the two phase-locking regions are well separated and a gap appears where the coupled-cavity lasers never lock. This gap increases with further increase of α [Fig. 6.22(e)] so that for $\alpha = 3$ there are two distinct phase-locking regions [Fig. 6.22(f)], one at low coupling-mirror transmissions $0 < T < 0.01$ and the other at relatively high coupling-mirror transmissions $0.45 < T < 1$. Furthermore, the generalized Hopf points H_g are gone and both phase-locking regions are again bounded by the entirely supercritical parts of S and H.

Bifurcations of Periodic Orbits

The next question concerns nonlinear oscillations for parameter settings within the gap between the two phase-locking regions. In a coupled-cavity laser periodic orbits emerge along Hopf bifurcation curves H, along curves S of global saddle-node homoclinic bifurcation, and along homoclinic bifurcation curves h. In particular, we already identified two types of codimension-two bifurcations, namely saddle-node-Hopf points $G_j^{\pm}$ and generalized Hopf points H_g. Both are sources of bifurcations of periodic orbits and, hence, starting

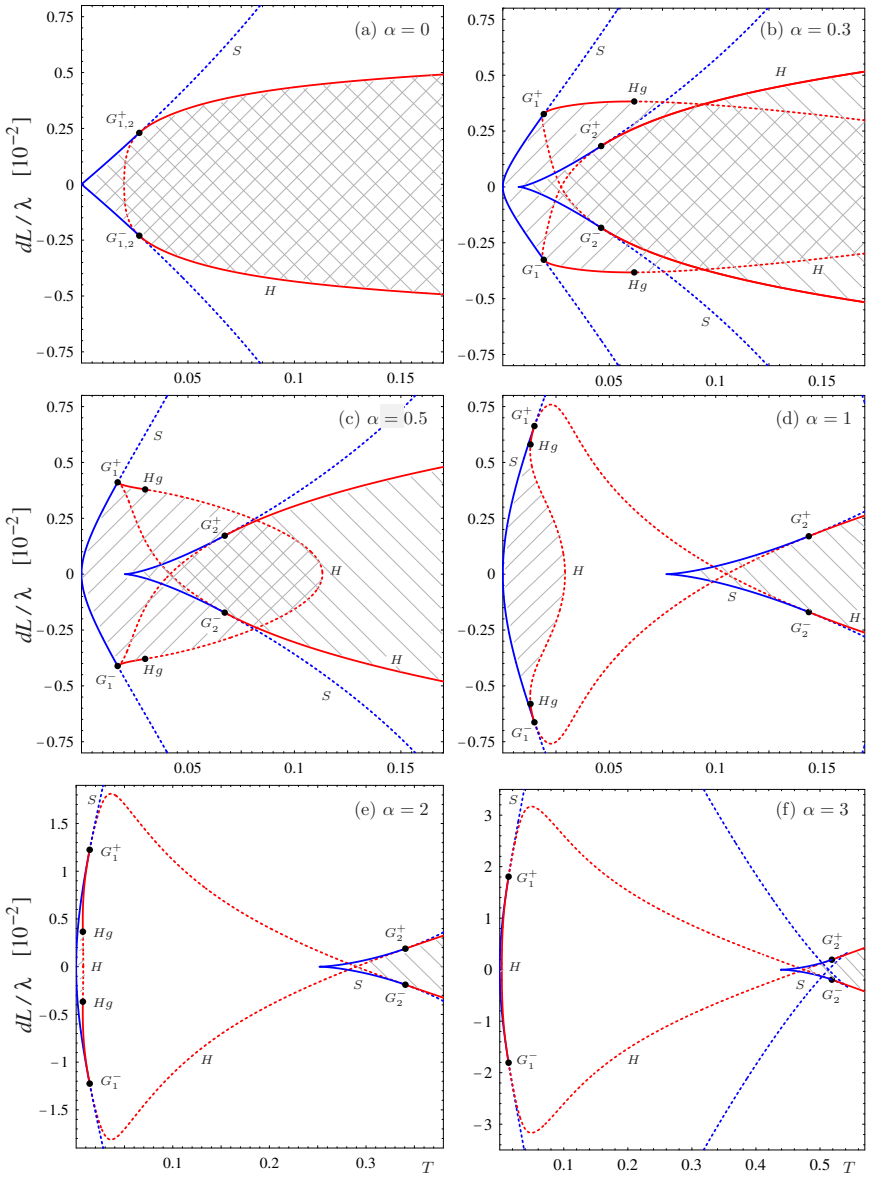

Fig. 6.22. Phase-locking region of (6.3)–(6.5) in the $(T, dL/\lambda)$-plane for different values of the linewidth enhancement factor α. S and H are tangent and change from supercritical to subcritical at codimension-two saddle-node-Hopf points $G^{\pm}_j$. H also changes from supercritical to subcritical at generalized Hopf points H_g. The color coding is as in Fig. 6.21. From S. Wieczorek and W.W. Chow, Global view of nonlinear dynamics in coupled-cavity lasers-a bifurcation study, *Opt. Comm.*, 246(4–6) (2005) 471–493 © 2004 by Elsevier Science; reprinted with permission.

points for further analysis. Note that in the plots of curves of bifurcations of periodic orbits we do not distinguish between super- and subcritical parts.

As expected from general theory [33], there is a torus bifurcation curve T emerging from each point $G_j^{\pm}$ [Fig. 6.23(a)]. Only two of four T curves are visible (since the case $\alpha = 0$ is degenerate). These torus curves involve two frequencies, the relaxation oscillation frequency and the inter-mode frequency. They are associated with a resonance tongue structure (not shown here) and denote the onset of either quasiperiodic (parameter settings between the tongues) or periodic oscillations (parameter settings within a resonance tongue) when the solid black curves T are crossed from the right to the left [38]. Also, they signal the appearance of chaos via the break-up of a 2-torus when the resonance tongues start to overlap. The curves T terminate at 1:2 resonance points [33, Sec. 9.5.3] where they connect to period-doubling curves PD^1. The PD^1 curves are the first steps in an infinite period-doubling cascade to chaos [18]. The secondary period-doubling curves $PD^{n>1}$ may be arranged in nested or unnested islands of period-doublings [61]. In either case, period-doubling islands are associated with chaotic dynamics. One of the period-doubling curves from Fig. 6.23(a) does not form a closed loop but terminates at two homoclinic-doubling bifurcation points B^1 [39]. Furthermore, there is a non-degenerate saddle-node-of-periodic-orbit curve SL where one of the two stable periodic orbits, born along the degenerate H curve, disappears. The overall dynamical picture for $\alpha = 0$ consists of the uninterrupted bistable phase-locking region and complicated, sometimes chaotic, dynamics found outside of the phase-locking region and near the points $G_j^{\pm}$.

When α is increased from zero [Fig. 6.23(b)], the degenerate bifurcation diagram unfolds and one clearly sees four torus curves connecting to period-doubling curves at four 1:2 resonance points. Interestingly, regions of complicated dynamics associated with $G_2^{\pm}$ start to overlap with the phase-locking region associated with $G_1^{\pm}$. There, depending on the initial condition, the coupled lasers may either be phase-locked or exhibit complicated unlocked oscillations. At the generalized Hopf points H_g, the curve SL attaches to the supercritical branches of H emerging from G_1^+ and G_1^-, causing the curves H to change from supercritical to subcritical. Stable periodic orbits born along these supercritical branches of H disappear at SL.

Increasing α further results in no qualitative changes to saddle-node Hopf points $G_2^{\pm}$ nor associated torus and period-doubling bifurcations. As the gap between the two phase-locking regions appears [Fig. 6.23(c)–(f)], the points $G_2^{\pm}$ move in the direction of higher values of T. Concurrently, the two torus curves T emerging from G_2^+ and G_2^- are 'dragged along', causing the two attached period-doubling cascades to shift into the gap between the two phase-locking regions. On the other hand, a number of qualitative changes takes place near $G_1^{\pm}$. For $\alpha < 0.5$, bifurcations of periodic orbits emerging from $G_1^{\pm}$ evolve in the direction of increasing $|dL/\lambda|$. Near $\alpha = 0.5$, the type of G_1^+ and G_1^- changes.

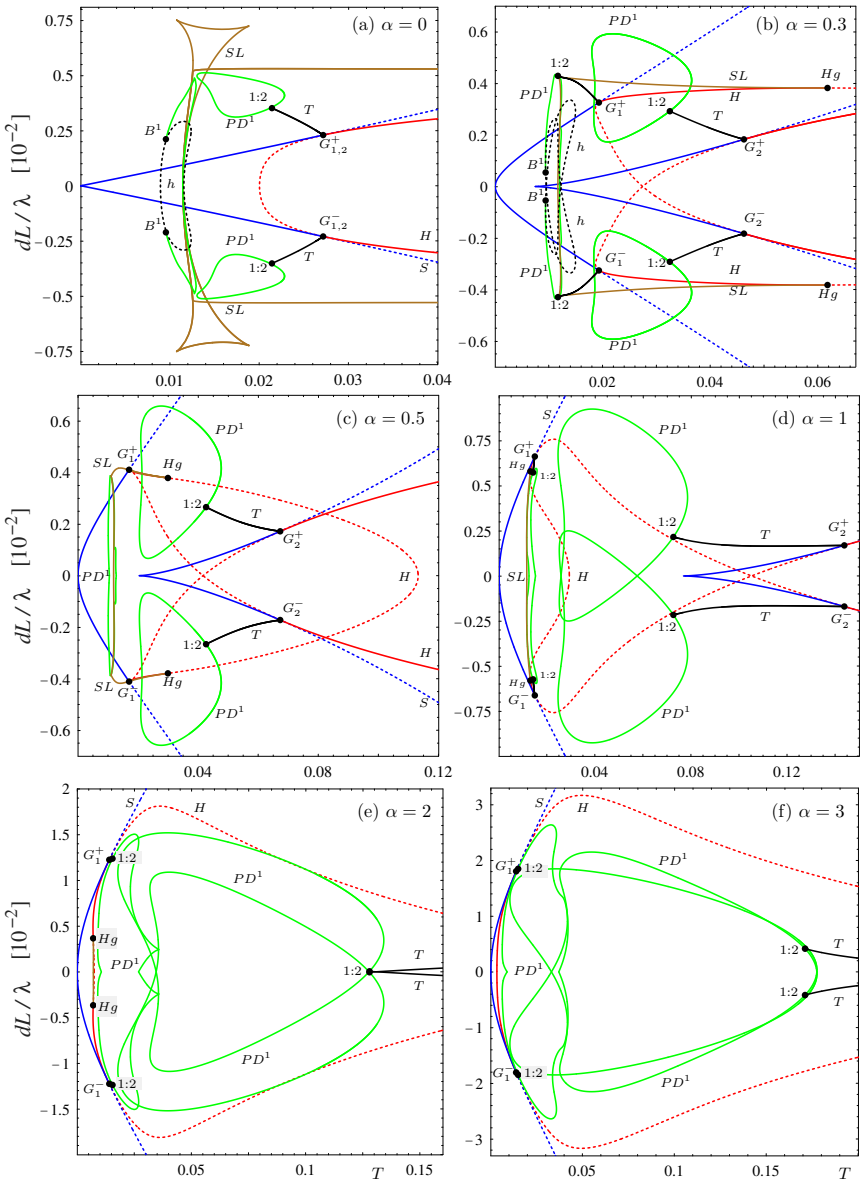

Fig. 6.23. Bifurcation diagram of (6.3)–(6.5) in the $(T, dL/\lambda)$ plane for different values of the linewidth enhancement factor α. Period-doubling bifurcation curves PD are in green, saddle-node bifurcation of periodic orbit curves SL are in brown, torus bifurcation curves T are in solid black, and homoclinic bifurcation curves h are in dotted black. From S. Wieczorek and W.W. Chow, Global view of nonlinear dynamics in coupled-cavity lasers-a bifurcation study, *Opt. Comm.*, 246(4–6) (2005) 471–493 © 2004 by Elsevier Science; reprinted with permission.

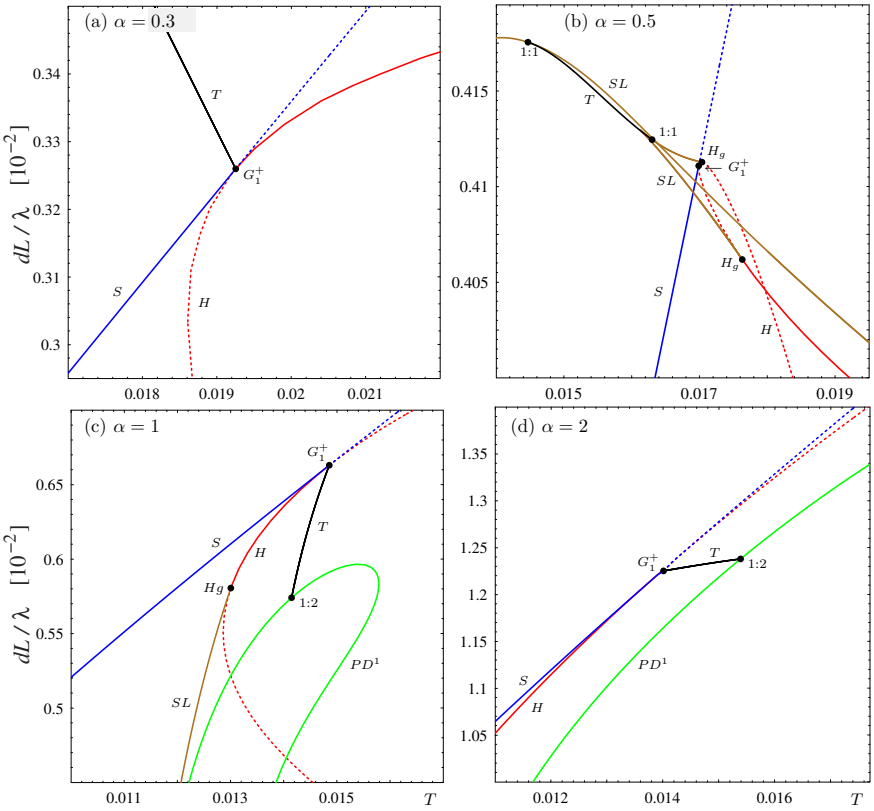

Fig. 6.24. Enlarged bifurcation diagram of (6.3)–(6.5) near saddle-node-Hopf point G_1^+ for different values of the linewidth enhancement factor α. From S. Wieczorek and W.W. Chow, Global view of nonlinear dynamics in coupled-cavity lasers-a bifurcation study, *Opt. Comm.*, 246(4–6) (2005) 471–493 © 2004 by Elsevier Science; reprinted with permission.

The details near G_1^+ are shown in Fig. 6.24. Close to $\alpha \simeq 0.5$ a new curve SL appears that connects to H at the two H_g points, and has a cusp near $(T, dL/\lambda) = (0.016, 0.4125)$ [Fig. 6.24(b)]. The torus curve T detaches from G_1^+ and attaches near the cusp of this new SL curve at 1:1 resonance [33, Sec. 9.5.2]. At $\alpha = 1$ [Fig. 6.24(b)] the extra SL curve is gone. The torus curve T attaches again to G_1^+ but 'flips' from above to below the curve S [Fig. 6.24(c)–(d)]. As a consequence, starting at $\alpha \simeq 1$ [Fig. 6.23(d)], the two torus curves T emerging from G_1^+ and G_1^-, and the attached period-doubling curves PD^1, start filling the gap between the two phase-locking regions [Fig. 6.23(d)–(f)]. For clarity, only parts of the PD^1 curves associated with G_1^+ and G_1^- are plotted in Fig. 6.23(b)–(f).

6.2.5 Concluding Remarks on Coupled Lasers

The interesting dynamics of coupled-cavity lasers arises from two types of nonlinearities: those imparted in the composite-mode properties by the optical coupling (algebraic constraints), and those imparted in the active medium by the population dynamics (differential equations). Their interplay results in a rich display of chaotic oscillations when two conditions are met simultaneously.

(i) The composite-cavity-mode beat note must be close to resonant with the characteristic (relaxation oscillation) frequency of the active medium, thus strongly coupling laser fields and active media;
(ii) an appreciable spatial overlap between composite-cavity modes must be present for a strong coupling of the lasing modes.

Continuation techniques allowed us to uncover a counter-intuitive example of chaos in ultra-weakly coupled nonlinear-oscillators and to explain how this unexpected dynamical picture arises with increasing linewidth enhancement factor α. In particular, an uninterrupted and degenerate (bistable) phase-locking region at $\alpha = 0$ unfolds and develops a gap, which is gradually occupied with instabilities and chaos for $\alpha \neq 0$. The underlying mechanism is a change in the competition between composite-cavity modes that causes a change in the type of codimension-two saddle-node Hopf points via a codimension-three cusp singularity on the Hopf bifurcation curve. Furthermore, several other codimension-two bifurcations, including strong resonances, are identified as sources of instabilities and chaos in coupled-cavity lasers. Many of the phenomena mentioned are interesting from a bifurcation theory point of view and should be studied in more detail.

The dependence of the dynamics on the cavity length reveals effects due to nonlinear optical coupling. With decreasing cavity length, the two conditions that are necessary for the complicated dynamics to occur shift towards the origin of the $(T, dL/\lambda)$ parameter space. Consequently, for short cavities these two conditions may be satisfied at ultra-low optical coupling (e.g. $T < 10^{-5}$ for $L \sim 3\lambda$), where lasers are generally expected to act independently. This bifurcation analysis provided new insight into an overall understanding of coupled-laser behavior.

6.3 Outlook

The field of nonlinear optical/laser systems is expanding in many new directions. Examples of new types of optical systems include nanoscale photonic-crystal lasers [41], optical resonators with quantum coherence [55, 67], and multimode quantum-dot lasers [49]. Owing to their nanoscale and quantum coherence, these systems are expected to have strong optical nonlinearities that are different from those found in conventional optical/laser systems. New

nonlinear phenomena are waiting to be uncovered and, based on our experience so far, we believe that continuation techniques are the tool of choice.

The nonlinear analysis of these newly emerging optical systems faces mathematical challenges such as handling high-dimensional multimode systems, ODEs with algebraic constraints, and multiple time scales. It is, therefore, an easy prediction that the bifurcation analysis of newly emerging problems in laser physics and photonics will continue to stimulate and contribute to the further development of continuation techniques themselves.

Acknowledgements

Individual results in this chapter have appeared in previous publications, and I thank my co-workers Bernd Krauskopf, Weng. W. Chow, and Daan Lenstra for their contributions. Text passages and figures have been reproduced with permission, and I thank the American Physical Society, Elsevier Science and Institute of Physics Publishing for permission to use material from [53], [54] and [58], respectively.

References

1. N. B. Abraham, L. A. Lugiato, and L. M. Narducci (Eds.), Special issue on Instabilities in Active Optical Media. *J. Opt. Soc. Am. B*, **2**, 1985.
2. A. Algaba, M. Merino, F. Fernández-Sánchez, and A. Rodriguez-Luis. Closed curves of global bifurcations in Chua's equations: a mechanism for their formation. *Internat. J. Bifurc. Chaos Appl. Sci. Engrg.*, **13**:609–616, 2002.
3. V. Annovazzi-Lodi, S. Donati, and M. Manna. Chaos and locking in a semiconductor laser due to external injection. *IEEE J. Quantum Electron.*, **30**(7):1537–1541, 1994.
4. A. Argyris, D. Syvridis, L. Larger, V. Annovazzi-Lodi, P. Colet, I. Fischer, J. Garcìa-Ojalvo, C. R. Mirasso, L. Pesquera, and K. A. Shore. Chaos-based communications at high bit rates using commercial fiber-optic links. *Nature*, **438**:343-346, 2005.
5. A. Back, J. Guckenheimer, M. R. Myers, F. J. Wicklin, and P. A. Worfolk. DsTool: Computer assisted exploration of dynamical systems. *Not. Amer. Math. Soc.*, **39**:303–309, 1992.
6. F. Bai and A. R. Champneys. Numerical computation of saddle-node homoclinic orbits of co-dimension one and two. *J. Dyn. Stab. Syst.*, **11**:325–346, 1996.
7. L. Belyakov. Bifurcation of systems with homoclinic curve of a saddle-focus with saddle quantity zero. *Mat. Zam.*, **36**:681–689, 1984.
8. P. Besnard, Private communication, 2006.
9. V. V. Bykov. The bifurcations of separatrix contours and chaos. *Physica D*, **62**(1-4): 290–299, 1993.
10. V. V. Bykov. Orbit structure in a neighborhood of a separatrix cycle containing two saddle foci in *Methods of qualitative theory if differential equations and related topics. American Math. Soc. Transl. Ser 2*, **200**:87–97, 2000.

11. A. R. Champneys and Yu. A. Kuznetsov. Numerical detection and continuation of codimension-two homoclinic bifurcations. *Internat. J. Bifurc. Chaos Appl. Sci. Engrg.*, **4**:785–822, 1994.
12. A. R. Champneys, Yu. A. Kuznetsov, and B. Sandstede. A numerical toolbox for homoclinic bifurcation analysis. *Internat. J. Bifurc. Chaos Appl. Sci. Engrg.*, **6**:867–887, 1996.
13. W. W. Chow. A composite-resonator mode description of coupled lasers. *IEEE J. Quant. Electron.*, **QE-22**(8):1174–1183, 1986.
14. S-N. Chow and X-B Lin. Bifurcation of a homoclinic orbit with a saddle-node equilibrium. *Diff. Int. Eqns.*, **3**:435–466, 1990.
15. B. Deng. Homoclinic bifurcations with nonhyperbolic equilibria. *SIAM J. Math. Anal.*, **21**:693–720, 1990.
16. E. Doedel, A. R. Champneys, T. Fairgrieve, Yu. A. Kuznetsov, B. Sandstede, and X. Wang. AUTO2000: Continuation and bifurcation software for ordinary differential equations. Available via http://indy.cs.concordia.ca/auto/main.html.
17. T. Erneux, V. Kovanis, A. Gavrielides, and P. M. Alsing. Mechanism for period-doubling bifurcation in a semiconductor laser subject to optical injection. *Phys. Rev. A*, **53**:4372–4380, 1996.
18. M. Feigenbaum. Quantitative universality for a class of nonlinear transformations. *J. Stat. Phys.*, **19**(1):25–52, 1978.
19. F. Fernández-Sánchez, E. Freire, and A. Rodriguez-Luis. T-points in a $\mathbb{Z}_2$-symmetric electronic oscillator:(I) analysis. *Nonlin. Dyn.*, **28**:53–69, 2002.
20. W. Forysiak, J. V. Moloney, and R.G . Harrison. Bifurcations of an optically pumped three-level laser model. *Physica D*, **53**(1):162–186, 1991.
21. A. Gavrielides, V. Kovanis, P. M. Varangis, T. Erneux, and G. Lythe. Coexisting periodic attractors in injection-locked diode lasers. *Quant. Semiclass. Opt.*, **9**:785–786, 1997.
22. P. Glendinning and C. Sparrow. T-points: A codimension two heteroclinic bifurcation. *J. Statist. Phys.*, **43**:479–488, 1986.
23. M. Golubitsky and D. G. Schaeffer, *Singularities and Groups in Bifurcation Theory, Vol. 1* Applied Mathematical Sciences **51** (New York:Springer).
24. S. V. Gonchenko, D. V. Turaev, P. Gaspard, and G. Nicolis. Complexity in the bifurcation structure of homoclinic loops to a saddle-focus. *Nonlinearity*, **10**:409–423, 1997.
25. D. Goulding and G. Huyet, Private communication, 2006.
26. K. Green, B. Krauskopf, and G. Samaey. A two-parameter study of the locking region of a semiconductor laser subject to phase-conjugate feedback. *SIAM J. Appl. Dyn. Sys.*, **2**(2):254–276, 2003.
27. A. J. Homburg. Periodic attractors strange attractors and hyperbolic dynamics near homoclinic orbits to saddle-focus equilibria. *Nonlinearity*, **15**:1029–1050, 2002.
28. D. M. Kane and K. A. Shore (Eds.), *Unlocking Dynamical Diversity: Optical Feedback Effects on Semiconductor Lasers*, (John Wiley & Sons, 2005).
29. V. Kovanis, A. Gavrielides, T. B. Simpson, and J.-M. Liu. Instabilities and chaos in optically injected semiconductor lasers. *Appl. Phys. Lett.*, **67**:2780–2782, 1985.
30. B. Krauskopf and D. Lenstra (Eds.), *Fundamental Issues of Nonlinear Laser Dynamics*, (AIP Conference Proceedings **548**, 2000).

31. B. Krauskopf, K. R. Schneider, J. Sieber, S. M. Wieczorek, and M. Wolfrum. Excitability and self-pulsations near homoclinic bifurcations in semiconductor laser systems. *Opt. Commun.*, **215**(4-6):367–379, 2003.
32. B. Krauskopf and J. Sieber. Bifurcation analysis of an inverted pendulum with delayed feedback control near a triple-zero eigenvalue singularity. *Nonlinearity*, **17**:85–103, 2004.
33. Yu. A. Kuznetsov, *Elements of Applied Bifurcation Theory*, (Springer, New York, 1995).
34. F.-Y. Lin and J.-M. Liu. Chaotic radar using nonlinear laser dynamics. *IEEE J. Quantum Electron.*, **40**(6):815–820, 2004.
35. L. A. Lugiato, L. M. Narducci, D. K. Bandy, and C. A. Pennise. Breathing spiking and chaos in a laser with injected signal. *Opt. Commun.*, **46**:64-68, 1983.
36. P. Mandel, *Theoretical Problems in Cavity Nonlinear Optics*, (Cambridge studies in modern optics, Cambridge University Press, 1997).
37. J. V. Moloney, J. S. Uppal, and R. G. Harrison. Origin of Chaotic Relaxation Oscillations in an Optically Pumped Molecular Laser. *Phys. Rev. Lett.*, **59**:2868–271, 1987.
38. E. Ott, *Chaos in Dynamical Systems* (Cambridge University Press, Cambridge, 1993).
39. B. Oldeman, B. Krauskopf, and A. R. Champneys. Death of period-doublings: locating the homoclinic-doubling cascade. *Physica D*, **146**:100–120, 2000.
40. I. M. Ovsyannikov and L. P. Shilnikov. Systems with a saddle-focus homoclinic curve. *Math. USSR-Sb.*, **58**(2):557–574, 1997.
41. B. Pasenow, M. Reichelt, T. Stroucken, T. Meier, S. W. Koch, A. R. Zakharian, and J. V. Moloney. Enhanced light-matter interaction in semiconductor heterostructures embedded in one-dimensional photonic crystals. *J. Opt. Soc. Am. B*, **22**(9):2039–2048, 2005.
42. M. Sargent III, M. O. Scully, and W. E. Lamb Jr., *Laser Physics*. (Addison-Wesley, 1974).
43. S. A. Shakir and W. W. Chow. Semiclassical theory of coupled lasers. *Opt. Lett.*, **9**:202–204, 1984.
44. M. V. Shashkov and D. V. Turaev. On the complex bifurcation set for a system with simple dynamics. *Internat. J. Bif. Chaos Appl. Sci. Engrg.*, **6**:949–968, 1996.
45. S. Schecter. Numerical computation of saddle-node homoclinic bifurcation points. *SIAM J. Numer. Anal.*, **30**(4):1155–1178, 1993.
46. J. Sieber. Numerical bifurcation analysis for multi-section semiconductor lasers. *SIAM J. Appl. Dyn. Syst.* **1**(2):248–270, 2002.
47. J. Sneyd, A. LeBeau, and D. Yule. Traveling waves of calcium in pancreatic acinar cells: model construction and bifurcation analysis. *Physica D*, **145**(1-2):158–179, 2000.
48. M. B. Spencer and W. E. Lamb Jr. Laser with a transmitting window. *Phys. Rev. A*, **5**(2):884–892, 1972.
49. Y. Tanguy, J. Houlihan, G. Huyet, E. A. Viktorov, and P. Mandel. Synchronization and clustering in a multimode quantum dot laser. *Phys. Rev. Lett.*, **96**(5):053902, 2006.
50. G. D. VanWiggeren and R. Roy. Communication with chaotic lasers. *Science*, **279**(5354):1198–1200, 1997.

51. C. O. Weiss and R. Vilaseca, *Dynamics of Lasers* (VCH Verlagsgesellschaft, Weinheim, Germany, 1991).
52. S. M. Wieczorek and W. W. Chow. Bifurcations and interacting modes in coupled lasers: A strong-coupling theory. *Phys. Rev. A*, **69**:033811, 2004.
53. S. M. Wieczorek and W. W. Chow. Chaos in practically-isolated microcavity lasers. *Phys. Rev. Lett.* **92**:213901, 2004.
54. S. M. Wieczorek and W. W. Chow. Global view of nonlinear dynamics in coupled-cavity lasers-a bifurcation study. *Opt. Commun.*, **246**(4-6):471–493, 2005.
55. S. M. Wieczorek and W. W. Chow. Self-induced chaos in a single-mode inversionless laser. *Phys. Rev. Lett.*, **97**:113903, 2006.
56. S. M. Wieczorek and W. W. Chow. On dynamical sensitivity of lasers and instability-based coherent-signal detection. submitted, 2007.
57. S. M. Wieczorek, W. W. Chow, L. Chrostowski, and C. J. Chang-Hasnain. Improved semiconductor-laser dynamics from induced population pulsation. *IEEE J. Quant. Electron.*, **QE-42**(6):552–562, 2006.
58. S. Wieczorek and B. Krauskopf. Bifurcations of n-homoclinic orbits in optically injected lasers. *Nonlinearity*, **18**:1095–1120, 2005.
59. S. M. Wieczorek, B. Krauskopf, and D. Lenstra. A unifying view of bifurcations in a semiconductor laser subject to optical injection. *Opt. Commun.*, **172**(1):279–295, 1999.
60. S. M. Wieczorek, B. Krauskopf, and D. Lenstra. Mechanisms for multistability in a semiconductor laser with optical injection. *Opt. Commun.*, **183**(1-4):215–226, 2000.
61. S. M. Wieczorek, B. Krauskopf, and D. Lenstra. Unnested islands of period-dublings in an injected semiconductor laser. *Phys. Rev. E*, **64**:056204, 2001.
62. S. M. Wieczorek, B. Krauskopf, and D. Lenstra. Multipulse excitability in a semiconductor laser with optical injection. *Phys. Rev. Lett.*, **88**:063901, 2002.
63. S. M. Wieczorek, B. Krauskopf, T. B. Simpson, and D. Lenstra. The dynamical complexity of optically injected semiconductor lasers. *Phys. Rep.*, **416**(1-2):1–128, 2005.
64. S. M. Wieczorek and D. Lenstra. Spontaneously excited pulses in an optically driven semiconductor laser. *Phys. Rev. E*, **69**:016218, 2004.
65. S. M. Wieczorek, T.B . Simpson, B. Krauskopf, and D. Lenstra. Global quantitative predictions of complex laser dynamics. *Phys. Rev. E*, **65**:045207R, 2001.
66. S. M. Wieczorek, T. B. Simpson, B. Krauskopf, and D. Lenstra. Bifurcation transitions in an optically injected diode laser: theory and experiment. *Opt. Commun.*, **215**(1-3):125–134, 2003.
67. W. Yang, A. Joshi, and M. Xiao. Chaos in an electromagnetically induced transparent medium inside an optical cavity. *Phys. Rev. Lett.*, **95**:093902, 2005.
68. M. G. Zimmermann, S. Firle, M. A. Natiello, M. Hildebrand, M. Eiswirth, M. Bar, A. K. Bangia, and I. G. Kevrekidis. Pulse bifurcation and transition to spatiotemporal chaos in an excitable reaction-diffusion model. *Physica D*, **110**(1-2):92–104, 1997.